

Flavor Dependence of Charged Pion Fragmentation Functions

H. Bhatt^a, P. Bosted^b, S. Jia^c, W. Armstrong^d, D. Dutta^a, R. Ent^e, D. Gaskell^e, E. Kinney^f, H. Mkrtchyan^g, S. Ali^h, R. Ambroseⁱ, D. Androic^j, C. Ayerbe Gayoso^a, A. Bandari^b, V. Berdnikov^h, D. Bhetuwal^a, D. Biswas^k, M. Boer^c, E. Brash^l, A. Camsonne^e, M. Cardona^c, J. P. Chen^e, J. Chen^b, M. Chen^m, E. M. Christy^k, S. Covrig^e, S. Danagoulianⁿ, M. Diefenthaler^e, B. Duran^c, M. Elaasar^o, C. Elliot^p, H. Fenker^e, E. Fuchey^q, J. O. Hansen^e, F. Hauenstein^r, T. Horn^h, G. M. Huberⁱ, M. K. Jones^e, M. L. Kabir^a, A. Karki^a, B. Karki^s, S. J. D. Kay^{h,t}, C. Keppel^e, V. Kumarⁱ, N. Lashley-Colthirst^k, W. B. Li^b, D. Mack^e, S. Malace^e, P. Markowitz^u, M. McCaughan^e, E. McClellan^e, D. Meekins^e, R. Michaels^e, A. Mkrtchyan^g, G. Niculescu^v, I. Niculescu^v, B. Pandey^{k,w}, S. Park^x, E. Pooser^e, B. Sawatzky^e, G. R. Smith^e, H. Szumila-Vance^{e,u}, A. S. Tadepalli^e, V. Tadevosyan^g, R. Trotta^h, H. Voskanyan^g, S. A. Wood^e, Z. Ye^{d,y}, C. Yero^u, X. Zheng^m

^aMississippi State University, Mississippi State, Mississippi, 39762, USA

^bThe College of William & Mary, Williamsburg, Virginia, 23185, USA

^cTemple University, Philadelphia, Pennsylvania, 19122, USA

^dArgonne National Laboratory, Lemont, Illinois, 60439, USA

^eThomas Jefferson National Accelerator Facility, Newport News, Virginia, 23606, USA

^fUniversity of Colorado Boulder, Boulder, Colorado, 80309, USA

^gA.I. Alikhanyan National Science Laboratory (Yerevan Physics Institute), Yerevan, 0036, Armenia

^hCatholic University of America, Washington, DC, 20064, USA

ⁱUniversity of Regina, Regina, Saskatchewan, S4S 0A2, Canada

^jUniversity of Zagreb, Zagreb, Croatia

^kHampton University, Hampton, Virginia, 23669, USA

^lChristopher Newport University, Newport News, Virginia, 23606, USA

^mUniversity of Virginia, Charlottesville, Virginia, 22903, USA

ⁿNorth Carolina A & T State University, Greensboro, North Carolina, 27411, USA

^oSouthern University at New Orleans, New Orleans, Louisiana, 70126, USA

^pUniversity of Tennessee Knoxville Tennessee, 37996, USA

^qUniversity of Connecticut, Storrs, Connecticut, 06269, USA

^rOld Dominion University, Norfolk, Virginia, 23529, USA

^sOhio University, Athens, Ohio, 45701, USA

^tUniversity of York, Heslington, York, YO10 5DD, UK

^uFlorida International University, University Park, Florida, 33199, USA

^vJames Madison University, Harrisonburg, Virginia, 22807, USA

^wVirginia Military Institute, Lexington, Virginia, 24450, USA

^xStony Brook University, Stony Brook, New York, 11794, USA

^yTsinghua University, Beijing, 100084, China

Abstract

We have measured the flavor dependence of multiplicities for π^+ and π^- production in semi-inclusive deep-inelastic scattering (SIDIS) on proton and deuteron to explore a possible charge symmetry violation in fragmentation functions. The experiment used an electron beam with energies of 10.2 and 10.6 GeV at Jefferson Lab and the Hall-C spectrometers. The electron kinematics spanned the range $0.3 < x < 0.6$, $2 < Q^2 < 5.5 \text{ GeV}^2$, and $2.2 < W < 3.2 \text{ GeV}$. The pion fractional momentum range was $0.3 < z < 0.7$, and the transverse momentum range was $0 < p_T < 0.25 \text{ GeV}/c$. Assuming factorization and allowing for isospin breaking, the results can be described by two “favored” and two “unfavored” effective low p_T fragmentation functions that are flavor-dependent. We find each pair converges to a common flavor-independent fragmentation function at the highest W , where factorization is most applicable.

Keywords: Charged pion multiplicities, fragmentation functions, charge symmetry violation, higher twist corrections

1. Introduction

Semi-inclusive deep-inelastic lepton-nucleon scattering ($IN \rightarrow l h X$) is an excellent tool to study the quark hadronization mechanism described by fragmentation functions (FF) [1]. These FF describe how the quarks and gluons (partons) transform into color-neutral hadrons or photons during high-energy (hard) scattering processes. Pion semi-inclusive deep-inelastic

scattering (SIDIS) is one such scattering process that allows access to the FF associated with the pions identified in the final state. These FF are the non-perturbative ingredient of the quantum chromodynamics (QCD) factorization theorems [2] used to analyze hard scattering processes and thereby provide insight into fundamental soft QCD quantities [3]. The FF are intimately connected to operator product expansion [4], with contributions from higher-order corrections that are suppressed

by the power of the hard scale. With the improving accuracy of recent and upcoming experiments, these so-called “higher twist” corrections, such as the hadron mass correction, are becoming increasingly important [5]. The FF are also intrinsically linked to confinement in QCD, hence studies of FF are critical for a complete understanding of the basic properties of QCD, such as the dynamical generation of the mass, spin, and size of hadrons [6].

The current knowledge of pion FF are based on global QCD analyses [7, 8, 9, 10, 11, 12, 13, 14] that are dominated by measurements from inclusive electron-positron (e^+e^-) annihilation into charged pions at very high energy scales (center-of-mass energy > 10 GeV). Inclusive e^+e^- annihilation is a clean process to study FF since it is independent of the parton distribution functions (PDF). However, it cannot distinguish between the light quark flavors or the quark and anti-quark FF. Thus, it cannot provide information about possible flavor dependence of FF – essential for a complete picture of FF and the spin structure of nucleons, in particular the transverse spin structure [15]. One of the most important advantages of SIDIS is the ability to constrain the flavor of the quark involved in the scattering process. Consequently, measuring the SIDIS process on the proton and deuteron allows an independent extraction of the flavor dependence of FF. The SIDIS experiments conducted over the last decade have convincingly established that the collinear picture of the quark-parton model is too simple, highlighting the importance of the transverse structure of the hadrons. The flavor structure of FF is important to understand the flavor dependence of the transverse-momentum-dependent (TMD) FF [15], and the relative differences between the observed single spin asymmetries of pions and kaons [16, 17]. Thus, SIDIS measurements provide a unique capability to study the flavor structure of FF at an energy scale that is complementary to that of e^+e^- annihilation.

It is challenging to model FF as they are non-perturbative objects that cannot be deduced from first principles. Current models treat hadronization either as the sequential emission of hadrons from colored partons with emission probability parameterized to describe experimental data, such as the Lund string model [18], or approximate it as the emission of a single hadron and an on-shell spectator quark [19]. Another recent approach combines these two methods by calculating the emission probability within a QCD-inspired spectator model instead of a parameterization [20]. As charge conjugation symmetry (CC) and charge/isospin symmetry (CS/IS) are fundamental properties of QCD, most models of strong interaction processes use a simple quark flavor-independent (for light quarks) and isospin-independent ansatz. At the quark level, CS refers to the up (u) and down (d) quark interactions being identical when their mass difference is neglected [21]. It arises from the invariance of the QCD Hamiltonian under rotations about the 2-axis in isospin space, i.e. the interchange of u and d quarks while simultaneously interchanging protons and neutrons [22]. Therefore, CC and CS/IS allow one to drastically reduce the number of independent FF for the light quarks from eight to two [4].

The FF are expected to respect CS/IS to high precision since the fragmentation process is a dominantly strong interaction

process. Most global fits of existing data that extract FF either assume CS or find no significant violation of CS [8, 9]. On the other hand, the transverse polarization of the Λ hyperon in e^+e^- annihilation, as measured by the Belle Collaboration [23], seems to indicate a significant IS violation in the corresponding FF. Further, a recent analysis of the results from the HERMES experiment [24] has reported a non-zero flavor dependence of FF [25], posing a significant challenge to QCD. These results and the quest for TMD FF have created an urgent need for a systematic study of the flavor dependence of FF and their charge (isospin) symmetry violation (CSV). Such studies are critical, as they enable the planned high precision hadron tomography studies at current [26] and future facilities, such as the Electron-Ion Collider [27]. They are also essential for unraveling the dynamics of the parton-to-hadron transition, which may reveal novel aspects of the emergent hadron mass [28, 29].

SIDIS is well suited for such studies, as the sum and difference ratio of π^+ and π^- production on proton to deuteron serves as an effective test of CS/IS. Further, the SIDIS reaction reflects higher twist contributions in the parton fragmentation sector, providing an effective tool to extract these contributions [30]. To exploit these advantages, a new SIDIS experimental program was undertaken at the upgraded JLab [31, 32, 33]. An integral part of this program, featuring measurements on both hydrogen (H) and deuterium (D) targets over a wide range of kinematics [31, 32], was completed in 2019. In this letter, we report the results of the tests of charge and isospin symmetry violation and flavor dependence of the unpolarized FF extracted from the SIDIS experimental program. Any flavor dependence of FF could indicate the importance of higher twist corrections and help determine their size when included in global fits. These results can also be significant for other parts of the SIDIS program, such as the test of CSV in PDF [31].

The p_T -integrated (p_T is the pion transverse momentum relative to the virtual-photon direction) semi-inclusive pion electroproduction yield ($\frac{dN}{dz}$) as a function of the pion’s longitudinal momentum fraction, z , is usually modeled as

$$\frac{dN}{dz} \sim \sum_i e_i^2 q_i(x, Q^2) D_{q_i \rightarrow \pi}(z, Q^2), \quad (1)$$

where the quarks of flavor i with charge e_i carrying a fraction x of nucleon momentum are represented by the PDF, $q_i(x, Q^2)$, and the spin averaged FF by $D_{q_i \rightarrow \pi}(z, Q^2)$. As a consequence of collinear factorization [2], the PDF are independent of z and FF are independent of x , but depend on the virtuality scale, or 4-momentum transferred squared (Q^2), via a logarithmic evolution [2, 34].

We define the measured multiplicities for π^+ and π^- production from proton (p) and deuteron (d), $M_{p/d}^{\pi^\pm}(x, Q^2, z)$, as the ratio of the respective SIDIS cross section to the inclusive DIS cross section. At leading order, assuming i) CS, ii) symmetric quark and anti-quark contributions from the sea, iii) identical p_T dependence of the measured multiplicities for charged pions from H/D targets, and iv) neglecting the strange quark contributions,

the sum and difference ratios simplify to,

$$R_1(z) = \frac{M_d^{\pi^+}(z) + M_d^{\pi^-}(z)}{M_p^{\pi^+}(z) + M_p^{\pi^-}(z)} = 1 \quad (2)$$

and

$$R_2(z) = \frac{M_d^{\pi^+}(z) - M_d^{\pi^-}(z)}{M_p^{\pi^+}(z) - M_p^{\pi^-}(z)} = \frac{3(4u(x) + d(x))}{5(4u(x) - d(x))}, \quad (3)$$

where the $u(d)$ quark PDF are written as $u(x) = u_v(x) + \bar{u}(x)$ and $d(x) = d_v(x) + \bar{d}(x)$, with $u_v(d_v)$ and $\bar{u}(\bar{d})$ as the valence quark and sea anti-quark contributions, respectively. For measurements made in the valence region ($x > 0.3$) where the contributions from the sea quarks can be neglected, both ratios are independent of z and p_T . Thereby, these two ratios constitute an excellent test of CS within the collinear factorization formalism [2].

Most global analyses to extract PDF assume IS and CS in the PDF [11, 8], which reduces the number of independent PDF by half. If we assume CS in the PDF but allow for non-zero CSV in FF, the multiplicity $M_{p/d}^{\pi^\pm}(x, Q^2, z)$ for each target (H/D) and charged pion type can be written in terms of two favored FF, $D_{u\pi^+}(z)$, $D_{d\pi^-}(z)$, and two unfavored FF, $D_{d\pi^+}(z)$, $D_{u\pi^-}(z)$, respectively (see Eq. S3 in the online Supplementary Material [35]). Any difference between the two favored and the two unfavored FF is an indication of CSV in FF. The degree of CSV in the favored and unfavored FF can be quantified in terms of two parameters defined as:

$$\delta_{\text{CSV}}^f(z) = \frac{D_{d\pi^-} - D_{u\pi^+}}{D_{u\pi^+}}, \quad \delta_{\text{CSV}}^{uf}(z) = \frac{D_{d\pi^+} - D_{u\pi^-}}{D_{u\pi^-}} \quad (4)$$

Most current global analyses to extract FF either impose exact CS or arrive at CSV parameters that are effectively zero.

We have measured the four multiplicities integrated over $0 < p_T < 0.25$ GeV/c, for the electroproduction of π^\pm from hydrogen and deuterium targets. These multiplicities, along with the PDF from a global fit of world data were used to extract the four FF. We have assumed an identical p_T dependence for the π^\pm multiplicities from proton and deuteron, integrated over p_T with an average of $\langle p_T \rangle = 0.1$ GeV/c. The CSV of FF are then quantified in terms of the two parameters in Eq. 4.

2. The experiment

The experiment was carried out in the Fall of 2018 and the Spring of 2019, in Hall C at JLab. The experiment used the quasi-continuous wave electron beam with beam energies of 10.2 and 10.6 GeV and beam currents ranging from 2 μA to 70 μA . The experimental yields were obtained from selected electron-pion coincidence events per milli-Coulomb of electrons incident on H, and D targets. The selected events passed cuts on momentum, scattering angles, and missing mass of the residual system, M_X , where M_X was restricted to be above the resonance region ($M_X > 1.6$ GeV/c²). The yields were integrated over the azimuthal angle (ϕ) and p_T with an average of $\langle p_T \rangle = 0.1$ GeV/c. The backgrounds from the target's aluminum windows and accidental coincidences were subtracted. This normalized SIDIS pion electroproduction yield

was corrected for all known inefficiencies of the two spectrometers such as the detector efficiencies (97%–99%), trigger efficiency (98%–99%), tracking efficiencies, computer and electronic live times (94%–99%). The corrected yields were binned in z for 8 different kinematic settings where the x ranged from 0.3 to 0.6, Q^2 ranged from 3.1 to 5.5 GeV² and the center-of-mass energy, W , ranged from 2.2 to 3.2 GeV. These ranges are complementary to previous experiments and constrained by the available maximum beam energy, the kinematic reach of the two spectrometers, and the desired statistical precision. A weighted average of settings with similar W and x reduced the 8 kinematic settings to 4.

A Monte Carlo (MC) simulation [36] of the SIDIS process was performed with the factorized form shown in Eq. 1. The CTEQ5 next-to-leading-order (NLO) PDF were used to parametrize $q(x, Q^2)$ [37] along with a parametrization of FF from fits of SIDIS data [38]. The MC was used to smear parameterized PDF and FF over the experimental acceptance. The MC included contributions due to radiative tails from exclusive pion electroproduction, pion and kaon decay, and electroproduction of ρ^0 mesons, and $\Delta(1232)$ resonances. Additional details about the models used in the simulation can be found in Refs. [39, 40, 41]. The MC yields were integrated over the same phase space as the measured yields. The diffractive ρ^0 contributions were subtracted from the experimental yields but they had negligible impact on the results extracted from these yields.

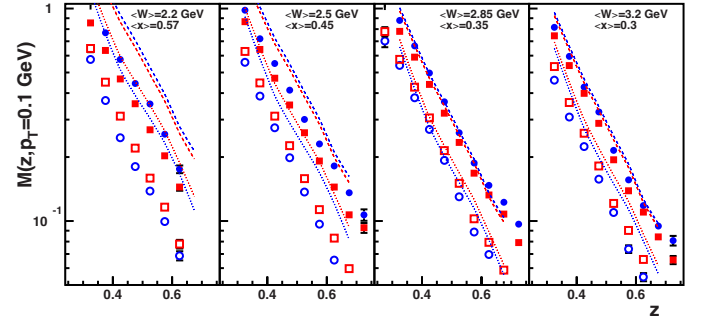


Figure 1: The z dependence of the four p_T -integrated charged pion multiplicities; $M_p^{\pi^+}$ ($M_d^{\pi^+}$) solid circles (squares) and $M_p^{\pi^-}$ ($M_d^{\pi^-}$) open circles (squares). The panels are ordered from left to right in increasing values of W . All curves are from global fits by the MAP [13, 42] collaboration integrated over the same p_T range as the experiment. The red (blue) dashed lines are for π^+ from H (D) target, while the dotted lines are for π^- .

3. Data analysis and results

The corrected experimental yields (as described in Sec. 2), the Monte Carlo yield, and the model cross section at $p_T = 0.1$ GeV/c were used to obtain the four multiplicities, $M_{p/d}^{\pi^\pm}(z)$ shown in Fig. 1. These results confirm that the p_T dependence for the π^\pm multiplicities from proton and deuteron are identical within the small p_T range covered, and the data agree better with global fits with increasing W . The sources of systematic uncertainty for the extracted multiplicities are listed in Table. 1,

Table 1: Systematic uncertainty of the multiplicities.

Source	Uncertainty (%)
Charge	0.45
Target related H (D)	0.8 (0.7)
Tracking & Live time	0.1
Particle identification	0.8
Background subtraction	0.2 - 2.0
Contamination	0.1
Acceptance	1.1
Kinematics	0.2
Radiative correction	1.1
Inclusive cross-section	2
FADC rate dependence	0.9
Total	3.0 - 3.6

and the total systematic uncertainty of 3.0 - 3.6 % is the quadrature sum of these uncertainties.

The uncertainty in the target density for H (D) includes contributions from the uncertainty in the target length, thermal contraction, temperature, pressure, and the equation of state used to calculate the target density. The beam currents were adjusted to keep the event rates for π^+ and π^- similar, ensuring that the particle identification efficiency for π^+ and π^- were similar within the uncertainty. The systematic uncertainty in the event selection arising from the particle identification cuts was determined from the average variation in the experimental yield when the cuts were varied by a small fixed amount (typically $\pm 10\%$ of the nominal values) and variation between multiple equivalent analyses of the same data set. The systematic uncertainty due to radiative correction was estimated from the average variation of the correction factor when the generation limits of the simulation of these radiative processes were varied and when the cross section models in the simulation were varied. The z correlated uncertainties in the models used to simulate Δ resonances, exclusive pion production, and ρ^0 meson production is the systematic uncertainty of the background subtraction procedure. They were estimated from the change in the simulated yield when the model parameters were varied. The systematic uncertainty due to the acceptance model in the Monte Carlo simulation was estimated from the variation of the multiplicity when the acceptance cuts were varied. The uncertainty in the inclusive cross section is from the latest fits to the world data [38]. Additional details about the experiment including how the systematic uncertainties were determined and their breakdown into different types are described in the Supplementary Material [35].

The four multiplicities were used to form the sum and difference ratios, which are shown as a function of z in Fig. 2 along with their statistical uncertainties. For the sum and difference ratios, many systematic uncertainties cancel to first order resulting in a net 2.2% systematic uncertainty shown by the magenta cross-hatched bands. The dotted lines are the expectations for models with CS/IS such as the fits by the JAM collaboration [11]. The dashed curves use FF from the global fits by the MAP [43] collaborations. The uncertainty for the JAM curves is not shown because, unlike the experiment and

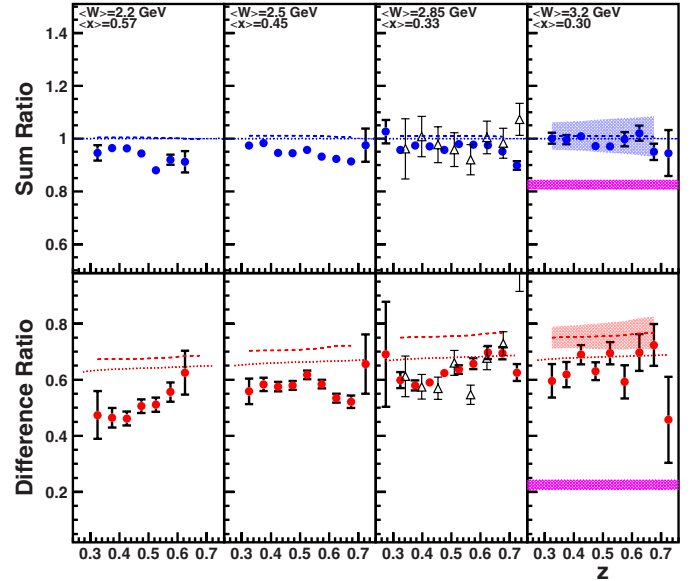


Figure 2: The ratios $R_1(z)$ (top panels) and $R_2(z)$ (bottom panels) as a function of z . The panels are ordered left to right in increasing values of W . The dotted lines are the JAM [11] predictions which assume CS/IS. The dashed curves and the hatched bands are the ratios and their uncertainty from the MAP [43] collaboration. The magenta cross-hatched bands show the 2.2% systematic uncertainty of these ratios. The open triangles in the third panels show the ratios obtained from the previous JLab 6 GeV experiment [34].

the MAP results, they are integrated over all p_T . At the highest W (3.2 GeV), the two ratios are remarkably independent of z over the entire range ($z = 0.3 - 0.7$) and are also consistent with the magnitude predicted by the global fits to existing data. In other words, the results agree with the CS/IS expectation. The sum ratio R_1 slowly but steadily deviates from the CS expectation with decreasing W (increasing x), both in terms of the z independence and the magnitude. Similarly, the difference ratio also shows increasingly large deviations from the CS expectation with decreasing W . These deviations may indicate the importance of higher twist contributions to the SIDIS cross sections at low W and the potential of these measurements to help determine the higher twist contributions. These results also indicate that even for the limited range of p_T covered in this experiment, CS/IS seems to be valid for $W > 3$ GeV. Moreover, the sum/difference ratio from the previous JLab 6 GeV experiment [34] (shown as black triangles in the third and sixth panel) agrees remarkably well with the current results. These older ratios were obtained at the same $x = 0.32$, but at significantly lower W and Q^2 of 2.4 GeV and 2.3 GeV², respectively. This seems to indicate that x may also be relevant for tests of CS/IS.

The four multiplicities were also used to obtain four FF ($D_{u\pi^+}(z)$, $D_{d\pi^-}(z)$ and $D_{u\pi^-}(z)$, $D_{d\pi^+}(z)$) by simultaneously solving a system of four equations as discussed earlier. The extracted FF are shown as a function of z in Fig. 3. Note that the JAM collaboration (solid lines) assumes CS/IS for all FF, while the DSS collaboration (dashed lines) assumes CS/IS only for the unfavored FF. The variation of the extracted FF due to the scale type uncertainties of the multiplicities and the accep-

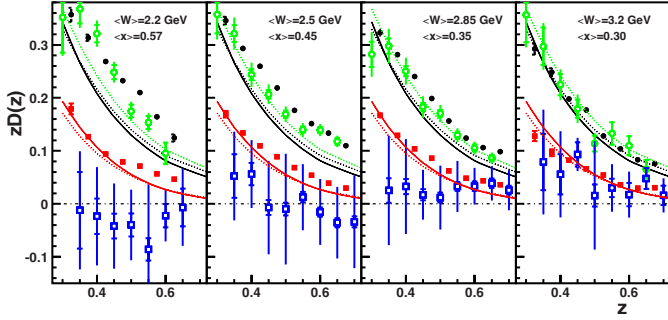


Figure 3: The z dependence of the two favored FF ($D_{u\pi^+}$ black solid and $D_{d\pi^-}$ green open, circles) and two unfavored FF ($D_{u\pi^-}$ red solid and $D_{d\pi^+}$ blue open, squares) extracted without assuming CS/IS. The panels are ordered left to right in increasing values of W . The inner error bars are the statistical uncertainty while the outer error bars are the total uncertainty. The solid (dashed) lines are FF from the JAM [11] (DSS [8, 9]) collaborations. The open points have been shifted in z for clarity.

tance cuts was used to determine the systematic uncertainty of the FF. The statistical and systematic uncertainty of the unfavored FF, $D_{d\pi^+}(z)$, is significantly larger than all the other FF, because it is determined by the small differences in the flavor-dependent multiplicities, which amplify the uncertainties. However, within these large uncertainties, it is consistent with zero. The large fluctuations permit unphysical negative values seen at low W .

The two favored and two unfavored FF were used to form the favored and unfavored $\delta_{CSV}(z)$ parameters as defined in Eq. 4 and are shown in Fig. 4. The variation in the δ_{CSV} parameter due to the choice of PDF and scale type uncertainty was used to determine the systematic uncertainties of δ_{CSV} . The shaded bands show the systematic uncertainty. The favored δ_{CSV} parameter is essentially zero within the experimental uncertainties over the entire range of z and W . They are also consistent with the expectations of the global fits by Peng and Ma [25] but not with the unconstrained fits by the MAP collaboration [43].

4. Discussion

The statistical uncertainties of the unfavored δ_{CSV} parameter are significantly larger than those for the favored. Within these larger uncertainties, the unfavored δ_{CSV} is consistent with zero at the highest W but deviates from zero with decreasing W (increasing x). These results and the sum and difference ratios shown in Fig. 2 are a direct experimental confirmation of CS/IS for both the favored and unfavored FF at the highest W . The results confirm that for $W > 3$ GeV ($x \leq 0.35$), where factorization is most applicable, the FF are flavor-independent, and the fragmentation process obeys CS/IS within experimental uncertainties. The results also show a more complex fragmentation process at lower W (higher x), with possible contributions from higher-order corrections. As these corrections can arise from quark-quark or quark-gluon correlations, they can be flavor dependent. These results provide an opportunity to help estimate the higher-order corrections.

The poor statistics in the unfavored down quark fragmentation channel drive the larger uncertainty in the unfavored CSV

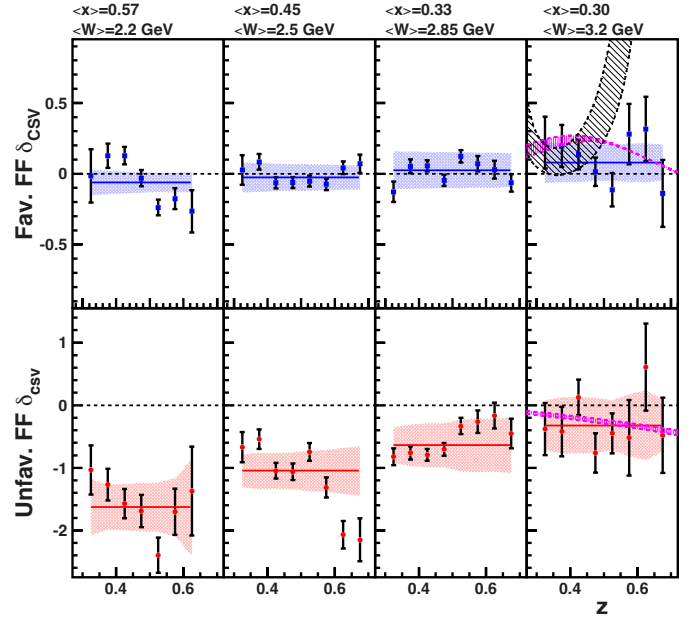


Figure 4: The z dependence of the CS/IS violating parameter δ_{CSV} for the favored FF (top panels) and unfavored FF (bottom panels). From left to right, the panels are ordered in decreasing values of x (increasing W). The blue (red) solid lines are constant value fits to δ_{CSV} . The shaded bands are the systematic uncertainty. The black dashed lines are expectations assuming CS ($\delta_{CSV} = 0$). In the last panels, the magenta band with vertical hatching is the δ_{CSV} and its uncertainty from Peng and Ma [25], while the black band with angled hatching is from the MAP collaboration [43].

parameter. Even in an isoscalar target, up quark scattering is a majority of the DIS cross section due to a larger electromagnetic coupling, and the poor statistics are exacerbated for SIDIS by the unfavored fragmentation configuration. Lacking a free neutron target, tagging the spectator ($A-1$) system would isolate hard scattering on the neutron. High-luminosity measurements with the spectator tagging of a proton or ^3He (using a D or ^4He target respectively) could significantly improve the uncertainties for unfavored down quark fragmentation.

5. Summary and outlook

In summary, we have measured the π^\pm multiplicities from SIDIS on H and D targets over a wide range of kinematics. The sum and difference ratios of the four multiplicities satisfy CS/IS at the highest W (3.2 GeV) but steadily deviate from the CS expectation with decreasing W (increasing x). The multiplicities were used to quantify the flavor dependence of FF, they confirm the flavor independence of both the favored and unfavored FF at the highest W . The favored FF are flavor independent, within uncertainties, over the W range of the experiment. Within the larger experimental uncertainty, the flavor dependence of the unfavored FF increases with decreasing W . The results also indicate that higher-twist corrections are important for low W . When these data are included in future global fits of PDF and FF including higher-order corrections, they will provide further detailed insight into the fragmentation process. These results also suggest that CSV in FF is unlikely to interfere with the forth-

coming extraction of CSV in PDF [31]. The spectator tagging technique pioneered at JLab can be used in future experiments to access nearly free neutron targets to improve the precision of the unfavored FF and their CSV.

6. Acknowledgements

This work was funded in part by the U.S. Department of Energy, including contract AC05-06OR23177 under which Jefferson Science Associates, LLC operates Thomas Jefferson National Accelerator Facility, and by the U.S. Department of Energy, Office of Science, contract numbers DE-AC02-06CH11357, DE-FG02-07ER41528, DE-FG02-96ER41003, and by the U.S. National Science Foundation grants PHY 2309976, 2012430 and 1714133 and the Natural Sciences and Engineering Research Council of Canada grant SAPIN-2021-00026. We wish to thank the staff of Jefferson Lab for their vital support throughout the experiment. We are also grateful to all granting agencies providing funding support to authors throughout this project.

References

- [1] R. D. Field, R. P. Feynman, *Phys. Rev. D* 15 (1977) 2590. doi:<https://doi.org/10.1103/PhysRevD.15.2590>.
- [2] J. C. Collins, D. E. Soper, G. Sterman, *Adv. Ser. Direct. High Energy Phys.* 5 (1988) 1. [link].
URL <https://arxiv.org/abs/hep-ph/0409313>
- [3] S. Albino, *Rev. Mod. Phys.* 82 (2010) 2489. doi:<https://doi.org/10.1103/RevModPhys.82.2489>.
- [4] A. Metz, A. Vossen, *Prog. in Part. and Nucl. Phys.* 91 (2016) 136–202. doi:<https://doi.org/10.1016/j.ppnp.2016.08.003>.
- [5] A. Acardi, T. Hobbs, W. Melnitchouk, *J. of High Eng. Phys.* 11 (2009) 84. doi:10.1088/1126-6708/2009/11/084.
- [6] A. Acardi, A. Signori, *Phys. Lett. B* 798 (2019) 134993. doi:<https://doi.org/10.1016/j.physletb.2019.134993>.
- [7] M. Hirai, S. Kumano, T. Nagai, K. Sudoh, *Phys. Rev. D* 75 (2007) 094009. doi:<https://doi.org/10.1103/PhysRevD.75.094009>.
- [8] D. deFlorian, R. Sassot, M. Stratmann, *Phys. Rev. D* 75 (2007) 114010. doi:<https://doi.org/10.1103/PhysRevD.75.114010>.
- [9] D. deFlorian, R. Sassot, M. Epele, R. J. Hernández-Pinto, M. Stratmann, *Phys. Rev. D* 91 (2015) 014035. doi:<https://doi.org/10.1103/PhysRevD.91.014035>.
- [10] S. Albino, B. Kniehl, G. Kramer, *Nucl. Phys. B* 803 (2008) 42–104. doi:<https://doi.org/10.1016/j.nuclphysb.2008.05.017>.
- [11] E. Moffat, W. Melnitchouk, T. C. Rogers, N. Sato, *Phys. Rev. D* 104 (2021) 016015. doi:<https://doi.org/10.1103/PhysRevD.104.016015>.
- [12] A. Bacchetta, V. Bertone, C. Bissolotti, G. Bozzi, M. Cerutti, F. Piacenza, M. Radici, A. Signori, *J. of High Eng. Phys.* 10 (2022) 127. doi:[https://doi.org/10.1007/JHEP10\(2022\)127](https://doi.org/10.1007/JHEP10(2022)127).
- [13] A. Bacchetta, V. Bertone, C. Bissolotti, G. Bozzi, M. Cerutti, F. Delcarro, M. Radici, L. Rossi, A. Signori, *J. of High Eng. Phys.* 08 (2024) 232. doi:[https://doi.org/10.1007/JHEP08\(2024\)232](https://doi.org/10.1007/JHEP08(2024)232).
- [14] M. Cerutti, L. Rossi, S. Venturini, A. Bacchetta, V. Bertone, C. Bissolotti, M. Radici, *Phys. Rev. D* 107 (2023) 014014. doi:<https://doi.org/10.1103/PhysRevD.107.014014>.
- [15] A. Signori, A. Bacchetta, M. Radici, G. Schnell, *J. of High Eng. Phys.* 11 (2013) 194. doi:[https://doi.org/10.1007/JHEP11\(2013\)194](https://doi.org/10.1007/JHEP11(2013)194).
- [16] A. Airapetian, et al., *Phys. Rev. Lett.* 103 (2009) 152002. doi:<https://doi.org/10.1103/PhysRevLett.103.152002>.
- [17] C. Adolph, et al., *Phys. Lett. B* 744 (2015) 250. doi:<https://doi.org/10.1016/j.physletb.2015.03.056>.
- [18] B. Andersson, G. Gustafson, G. Ingelman, T. Sjöstrand, *Phys. Reports* 97 (1983) 31. doi:[https://doi.org/10.1016/0370-1573\(83\)90080-7](https://doi.org/10.1016/0370-1573(83)90080-7).
- [19] P. Mulders, R. Tangerman, *Nucl. Phys. B* 461 (1996) 197. doi:[https://doi.org/10.1016/0550-3213\(95\)00632-X](https://doi.org/10.1016/0550-3213(95)00632-X).
- [20] T. Ito, *Phys. Rev. D* 80 (2009) 074008. doi:<https://doi.org/10.1103/PhysRevD.80.074008>.
- [21] G. Miller, B. Nefkens, I. Šlaus, Charge symmetry, quarks and mesons, *Phys. Rep.* 194 (1990) 1. doi:[https://doi.org/10.1016/0370-1573\(90\)90102-8](https://doi.org/10.1016/0370-1573(90)90102-8).
- [22] J. T. Londergan, S. Braendler, A. W. Thomas, *Phys. Lett. B* 424 (1998) 185. doi:[https://doi.org/10.1016/S0370-2693\(97\)01483-4](https://doi.org/10.1016/S0370-2693(97)01483-4).
- [23] Y. Guan, et al., *Phys. Rev. Lett.* 122 (2019) 042001. doi:<https://doi.org/10.1103/PhysRevLett.122.042001>.
- [24] A. Airapetian, et al., *Phys. Rev. D* 87 (2013) 074029. doi:<https://doi.org/10.1103/PhysRevD.87.074029>.
- [25] Q. Peng, B.-Q. Ma, *Phys. Rev. C* 107 (2023) 055202. doi:<https://link.aps.org/doi/10.1103/PhysRevC.107.055202>.
- [26] J. Dudek, et al., *Eur. Phys. J. A* 48 (2012) 187. [link].
URL <https://link.springer.com/article/10.1140/epja/i2012-12187-1>
- [27] A. Acardi, et al., *Eur. Phys. J. A* 52 (2016) 268. [link].
URL <https://link.springer.com/article/10.1140/epja/i2016-16268-9>
- [28] H. Y. Xing, Z. Q. Yao, B. L. Li, D. Binos, Z. F. Cui, C. D. Roberts, *Eur. Phys. Jour. C* 84 (2024) 82. doi:<https://doi.org/10.1140/epjc/s10052-024-12403-7>.
- [29] C. D. Roberts, D. G. Richards, T. Horn, L. Chang, *Prog. Part. Nucl. Phys.* 120 (2021) 103883. doi:<https://doi.org/10.1016/j.ppnp.2021.103883>.
- [30] G. Xu, E. Hungerford, L. Pinsky (2005). [link].
URL <https://arxiv.org/abs/nucl-th/0505060>
- [31] K. Hafidi, D. Gaskell, D. Dutta, et al., jefferson Lab experiment E12-09-002. [link].
URL https://www.jlab.org/exp_prog/proposals/09/PR12-09-002.pdf
- [32] H. Mkrtchyan, P. Bosted, R. Ent, E. Kinney, et al., jefferson Lab experiment E12-09-017. [link].
URL https://www.jlab.org/exp_prog/proposals/proposal_updates/E12-09-017_Update_pac38.pdf
- [33] H. Avakian, et al., the CLAS12 collaboration, Run groups A and B. [link].
URL https://www.jlab.org/exp_prog/proposals/06/PR12-06-112.pdf
- [34] T. Navasardyan, et al., *Phys. Rev. Lett.* 98 (2007) 022001. doi:<https://doi.org/10.1103/PhysRevLett.98.022001>.
- [35] See, Supplementary Material for a description of the experimental details including kinematic settings, data analysis methods, and systematic uncertainties.
- [36] https://hallcweb.jlab.org/wiki/index.php/SIMC_Monte_Carlo.
- [37] H. L. Lai, et al., *Phys. Rev. D* 55 (1997) 1280. doi:<https://doi.org/10.1103/PhysRevD.55.1280>.
- [38] P. E. Bosted, M. E. Christy, *Phys. Rev. C* 77 (2008) 065206. doi:<https://doi.org/10.1103/PhysRevC.77.065206>.
- [39] H. Bhatt, PhD Dissertation, Mississippi State University, 2023. [link].
URL <https://misportal.jlab.org/sti/publications/23431>
- [40] S. Jia, PhD Dissertation, Temple University, 2022. [link].
URL <https://misportal.jlab.org/sti/publications/21868>
- [41] P. Bosted, et al., Transverse momentum and azimuthal dependence of charged pion multiplicities, publication in preparation.
- [42] M. Cerutti, private communications, 2024.
- [43] LHAPDF. [link].
URL <https://www.lhapdf.org>

Supplementary Material for Flavor Dependence of Charged Pion Fragmentation Functions

S-I. The Experiment

The experiment was carried out in Hall C at Jefferson Lab using a quasi-continuous wave electron beam with energies of 10.2 to 10.6 GeV and beam currents ranging from $2 \mu\text{A}$ to $70 \mu\text{A}$. The beam energy was measured with $< 0.05\%$ relative uncertainty from the bend angle of the beam as it traversed a set of magnets with precisely known field integrals. The total accumulated beam charge was determined using a set of resonant-cavity based beam-current monitors and a parametric transformer as gain monitor. The relative uncertainty of the accumulated beam charge was $\approx 0.5\%$, after correcting for zero-offsets and saturation effects measured using beam current scans on a solid carbon target. The beam was rastered at $\approx 25 \text{ kHz}$ over a $2 \times 2 \text{ mm}^2$ square pattern to minimize density reduction in the target due to localized beam heating.

The main production targets were a 10-cm-long (726 mg/cm^2) liquid hydrogen (H) and a 10-cm-long (1690 mg/cm^2) liquid deuterium (D) targets. Two aluminum foils placed 10-cm apart were used to determine the background from the aluminum entrance ($\approx 14 \text{ mg/cm}^2$) and exit ($\approx 19 \text{ mg/cm}^2$) end caps of the cryogenic target cells. A small reduction in density due to localized beam heating was determined to be $-0.023\%/\mu\text{A}$ for the liquid hydrogen target and $-0.027\%/\mu\text{A}$ for the liquid deuterium target.

Table S1: The eight kinematic settings where data were collected on both hydrogen and deuterium targets. The settings (1,2), (3,4,5), and (6,7), which have similar W and x were averaged for all the plots shown in the main article.

Setting	Ebeam (GeV)	E' (GeV/c)	θ_e (deg)	Q^2 (GeV ²)	W (GeV)	x	p_π (GeV/c)	θ_π (deg)
1	10.2	5.240	18.51	5.5	2.2	0.59	2.219, 2.713, 3.208	17.75
2	10.6	5.971	15.75	4.8	2.2	0.55	1.838, 2.299, 2.761, 3.223	18.55
3	10.6	5.971	14.24	3.9	2.4	0.45	1.838, 2.299, 2.761, 3.223	17.04
4	10.6	5.240	16.30	4.5	2.5	0.45	2.525, 3.363, 5.04	8-26
5	10.6	4.945	17.26	4.7	2.6	0.44	2.241, 2.804, 3.366, 3.928	14.16
6	10.6	5.240	13.50	3.1	2.8	0.31	1.956, 2.575, 3.433, 4.79	8-30
7	10.6	4.483	16.64	4.0	2.9	0.35	2.428, 3.037, 3.646, 4.234	11.61
8	10.6	3.307	19.70	4.1	3.2	0.30	2.645, 3.393, 4.531, 6.786	8-22

Scattered electrons were detected in the High Momentum Spectrometer [S1] in coincidence with charged pions detected in the Super High Momentum Spectrometer [S2]. The angle and momentum of the electron arm (13 - 49 deg., 1 - 6 GeV/c) and the hadron arm (6 - 30 deg., 2 - 7 GeV/c) were chosen to map the region between $0.2 \leq x \leq 0.6$ and $0.3 \leq z \leq 0.7$, where x is the fraction of nucleon momentum carried by the struck quark, and z is the pion's longitudinal momentum fraction. The angle, θ_{pq} , between the electron three-momentum transfer, \vec{q} and the hadron momentum, was chosen to cover a range in pion transverse momentum p_T up to 0.25 GeV/c. The kinematics of the experiment are complementary to that of previous experiments and are listed in Table S1. The number of good $e - \pi^+$ and $e - \pi^-$ events from the H (D) target ranged from $\sim 180,000$ (213,000) and 80,000 (107,000) at the lowest Q^2 (3.1 GeV²) to 4,000 (10,000) and 2,300 (9,000) at the highest Q^2 (5.5 GeV²).

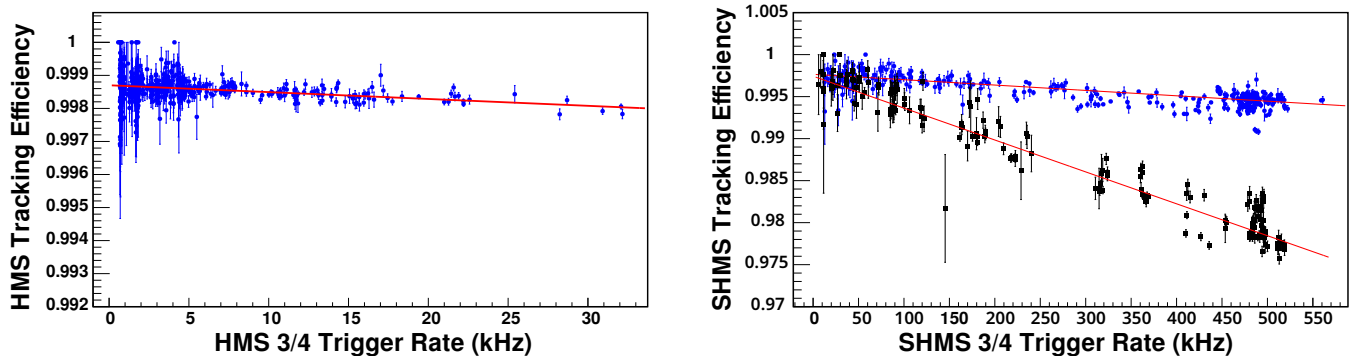


Figure S1: The tracking efficiency of the HMS (left) and SHMS (right) drift chambers as a function of the 3/4 trigger rate. The rate dependence of the efficiency is fit to a first order polynomial. For the HMS, the χ^2 per degree of freedom is 1.2. For the SHMS, the χ^2 per degree of freedom is 7.9 for the Spring 2018 (black squares) and 1.2 for the Fall 2019 (blue circles) run periods. The tracking efficiency corrections were applied run-by-run and only the statistical uncertainties are shown.

The detector packages of the two spectrometers are similar, and they included four segmented planes of plastic scintillators (except for the last plane in the SHMS, which used quartz bars) that were used to form the trigger in order to read out the time and amplitude signals from all of the detectors. To ensure nearly 100% efficiency for the triggers, signals from any three out of the four planes in each spectrometer were required. Henceforth referred to as the 3/4 trigger for each spectrometer. The time resolution of each plane was about 0.5 nsec, resulting in an accuracy of typically 0.3 nsec when all four planes were combined. Two drift chambers, each containing six planes of wires oriented at 0° and $\pm 60^\circ$ with respect to the horizontal, provided position and direction (track) information at the spectrometer focal plane with a resolution of $<250 \mu\text{m}$. The track information was used to reconstruct the momentum and the angle of the particle at the target (reaction vertex). After many improvements to the tracking software, the tracking efficiency in the HMS was determined to be over 99.7% throughout the experiment as shown in Fig. S1 (left). For the SHMS, the tracking efficiency varied between 99.5% at low trigger rates to 98% at the highest trigger rate. The rate dependence of the tracking efficiency was slightly different between the Spring 2018 and Fall 2019 run periods, as shown in Fig. S1 (right).

In the HMS (the electron spectrometer), a threshold gas Cherenkov detector and a segmented Pb-glass calorimeter [S1] were used for electron identification. A constant efficiency of 98% was estimated for the Cherenkov detector in the HMS, as shown in Fig. S2 (left). The efficiency of the HMS calorimeter was $\sim 99\%$ throughout the experiment as shown in Fig. S2 (right).

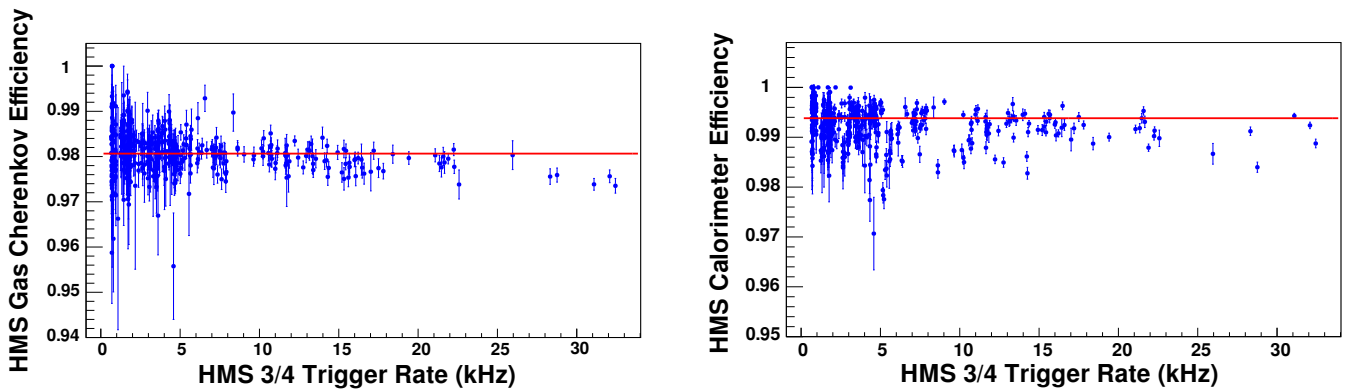


Figure S2: The HMS gas Cherenkov efficiency (left) and the HMS calorimeter efficiency (right) as a function of HMS 3/4 trigger rate. The solid lines show the constant value fits for each, with a χ^2 per degree-of-freedom of 1.7 and 9.9, respectively. For the HMS gas Cherenkov, a constant value of 0.98 was used as the correction factor, while a constant value of 0.994 was used for the calorimeter. Only the statistical uncertainties are shown.

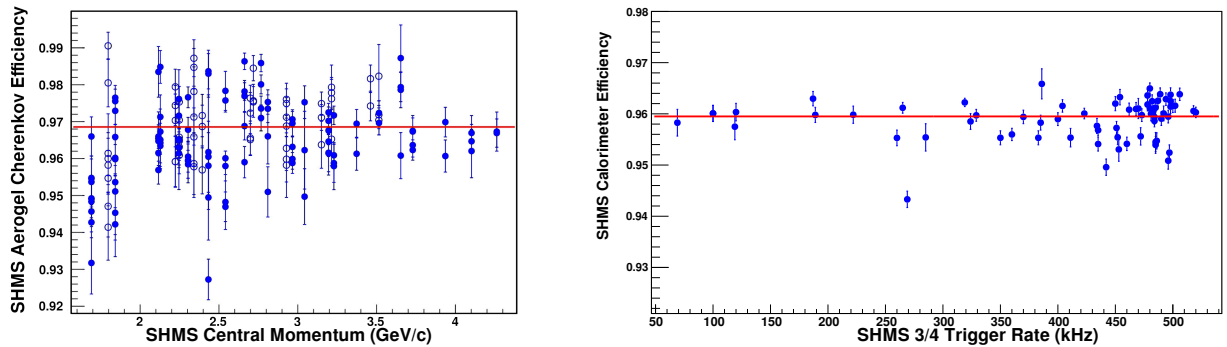


Figure S3: (left) The pion identification efficiency of the SHMS aerogel detector as a function of the pion momentum for π^+ (solid) and π^- (open). (right) The SHMS calorimeter efficiency as a function of 3/4 trigger rate (π^+). The solid lines are constant values fits that were used as the efficiency corrections. Only the statistical uncertainties are shown.

The pions in the SHMS (the hadron spectrometer) were identified using the electron-hadron coincidence time, the heavy-gas ($\text{C}_4\text{F}_8\text{O}$ at less than 1 atm. pressure) threshold Cherenkov detector, the aerogel Cherenkov detector [S3], and a segmented Pb-glass calorimeter [S1]. The pion identification efficiency of the aerogel Cherenkov varied between 94% for low momentum ($< 2 \text{ GeV}/c$) pions to 97% for the highest momentum pions as shown in Fig. S3 (left). The SHMS calorimeter efficiency was $\sim 96\%$ as shown in Fig. S3 (right). The heavy-gas threshold Cherenkov detector had an inefficient region near the center of the detector. The events from this inefficient region were removed from the analysis using a geometric cut as shown in Fig. S4 (left). The efficiency of the heavy-gas Cherenkov detector above the pion threshold, after removing events from the inefficient region, is shown in Fig. S4 (right). The Monte Carlo (MC) simulation of the experiment was used to determine and correct for the small contamination due to

pions generated from the decay of kaons. Moreover, the beam currents were adjusted to keep the event rates for π^+ and π^- similar, ensuring that the particle identification efficiency for π^+ and π^- were similar within the uncertainty.

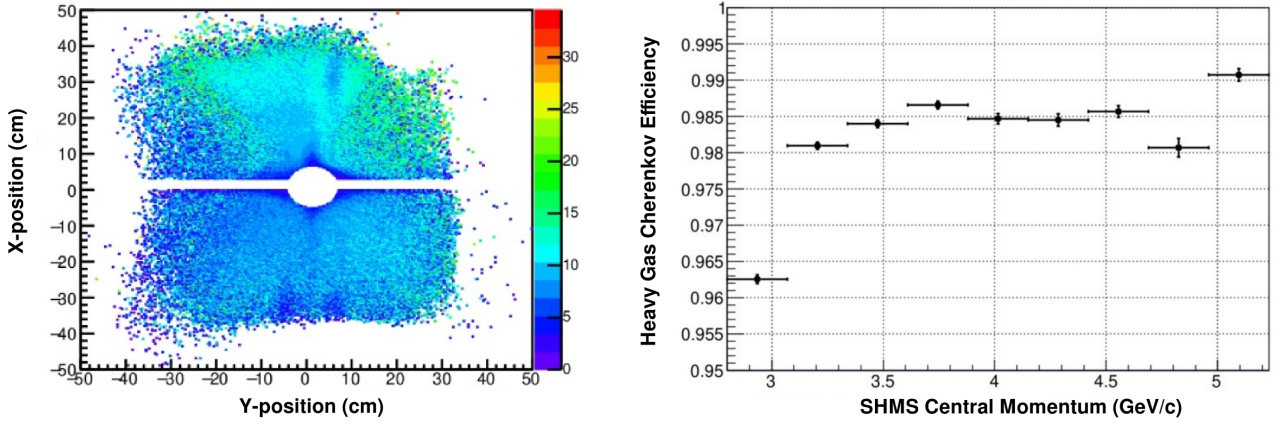


Figure S4: (left) The x-position vs. y-position of hits on the heavy-gas Cherenkov detector, showing the inefficient region of the Cherenkov detector that was removed from the analysis. The color bar represents the number of photo-electrons. (right) The charged pion efficiency of the heavy-gas Cherenkov detector as a function of the SHMS momentum.

In addition, the radio-frequency (RF) time information provided for each beam bucket along with electron-hadron coincidence time was also used for particle identification. The purity of the pion sample was determined using the RF timing information with and without constraints from the heavy-gas Cherenkov, as shown in Fig. S5 (left) for the positive pions. Events with positive pion momenta above 2.8 GeV/c have significant kaon contamination when not suppressed by the constraint from the heavy-gas Cherenkov detector. This contamination was negligible for negative pions. In this analysis, the heavy-gas Cherenkov was used to suppress kaons and the yields were corrected for contamination. The difference in the extracted multiplicity, with kaon rejection using the heavy-gas Cherenkov or with a correction to the pion purity without using the heavy-gas Cherenkov, was used to determine the systematic uncertainty due to kaon contamination of the pion sample. This difference was negligible for negative pions. The efficiency of the RF constraint as a function of SHMS momentum is shown in Fig. S5 (right) for π^+ (blue squares) and π^- (red circles).

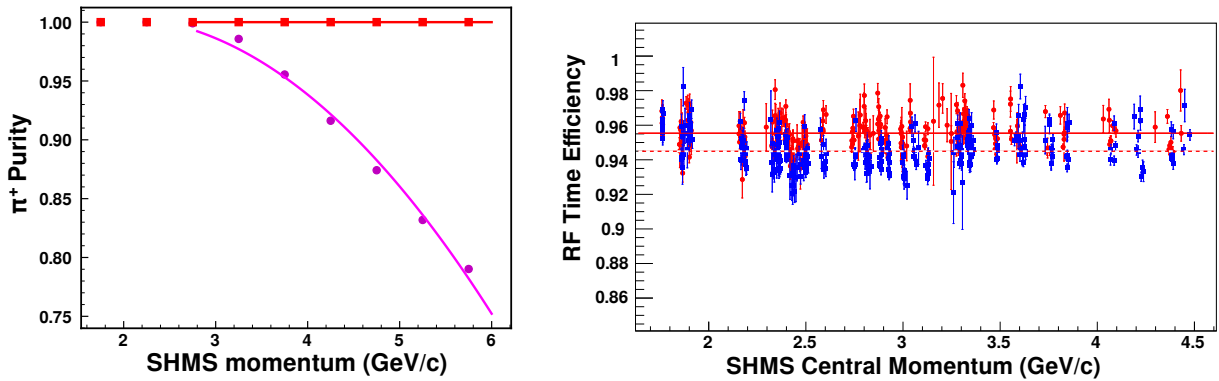


Figure S5: (left) The purity of the pion sample with (red squares) and without (magenta circles) constraints from the heavy-gas Cherenkov as a function of the pion momentum. (right) The RF time efficiency of the π^+ (blue squares) and π^- (red circles) as a function of SHMS central momentum. The lines are the constant value fits for π^+ (dotted) and π^- (solid) with χ^2 per degree of freedom 3.86 and 6.21 respectively. A constant value of 0.95 was used as the RF time efficiency throughout the experiment. Only the statistical uncertainties are shown.

The electron-pion coincidence events were recorded in approximately 1-hour-long runs via a data acquisition system operated using the CEBAF Online Data Acquisition (CODA) software package [S4]. The accidental backgrounds were subtracted by sampling the accidental events corresponding to several adjacent beam buckets on either side of the true coincident events. Prescaled singles (inclusive) electron and proton events were simultaneously recorded for systematic studies.

Data collected on the two aluminum foil targets were used to subtract the events from the aluminum walls of the cryogenic target cell. The background from π^0 production, subsequent decay and eventual conversion to electron-positron pairs was determined to

be negligible (< 1% of yield in the worst case) based on representative data collected by detecting positrons in the HMS. The total

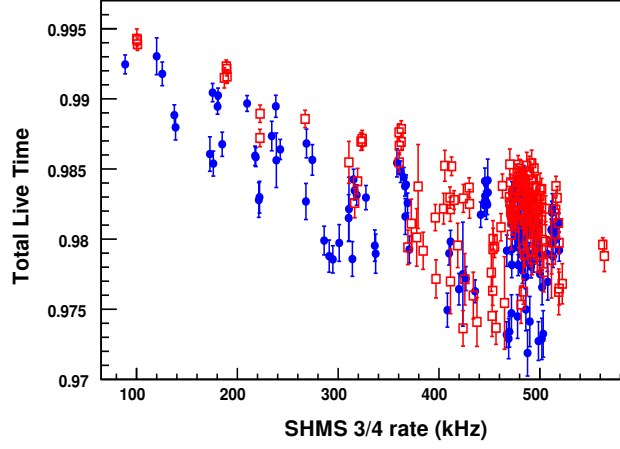


Figure S6: The total live time of the π^+ (red open squares) and π^- (blue circles) events as a function of the trigger rate in the SHMS which was the hadron spectrometer. Only the statistical uncertainties are shown.

live-time (product of the electronic and computer live-times) of the data acquisition (DAQ) system was measured using a special trigger called an Electronic Dead Time Monitor (EDTM). The EDTM consists of a known, fixed-frequency trigger, deliberately chosen to be a low rate (10 Hz in this experiment) such that it does not block the real trigger. The ratio of the recorded to the expected EDTM triggers was used as the total live-time of the DAQ. The total live time plotted as a function of the hadron trigger rate in the SHMS spectrometer is shown in Fig. S6.

S-II. Data Analysis

The charge-normalized and background subtracted coincidence yield on the H and D targets were obtained by integrating over the experimental phase space, including azimuthal angle ϕ and p_T . This normalized SIDIS pion electroproduction yield was corrected for the live-time and all the inefficiencies listed earlier and binned in z . The corrected yield, along with yields from the Monte Carlo simulation, was used to extract the multiplicity, defined as the ratio of the SIDIS cross section to the inclusive DIS cross section for each target nucleus (p/d) and charged pion type, given by:

$$M_{p/d}^{\pi^\pm}(x, Q^2, z) = \frac{d\sigma_{ee'\pi X}}{d\sigma_{ee'X}} = \frac{\sum_i e_i^2 q_i^{p/d}(x) D_{q_i \rightarrow \pi^\pm}(z)}{\sum_i e_i^2 q_i^{p/d}(x)}, \quad (\text{S1})$$

where $q_i^{p/d}(x)$ is the parton distribution function for quarks of flavor i , and charge e_i , in proton (p) or deuteron (d) as a function of Bjorken x . $D_{q_i \rightarrow \pi^\pm}(z)$ is the fragmentation function that represents the probability density for a quark of flavor i to fragment into a charged pion.

The inclusive DIS cross section is from a phenomenological model that uses all available data on inclusive DIS. Data collected at the kinematic settings used for this paper were shown to be consistent with this model. It is the most comprehensive model of the DIS cross section measured with the electron spectrometer used in this experiment. The dead time monitoring scheme used in this experiment was accurate only for the primary coincidence trigger and was less reliable for extracting the inclusive cross sections from our data. Using the fit to the world data on inclusive cross sections was determined to be the more reliable approach.

The four multiplicities at different values of z are shown as a function of W^2 in Fig. S7. The four multiplicities show the expected z dependence (i.e decreasing monotonically with increasing z). They also show an increase in the slope of the W^2 dependence as the z increases.

Assuming charge symmetry for PDF but not for the fragmentation functions (FF), the multiplicity $M_{p/d}^{\pi^\pm}(x, Q^2, z)$ can be ex-

panded in terms of the quark content of the two targets as:

$$\begin{aligned}
M_p^{\pi^+}(x, Q^2, z) &= \frac{4u(x)D_{u\pi^+}(z) + \bar{d}(x)D_{d\pi^+}(z)}{4u(x) + 4\bar{u}(x) + d(x) + \bar{d}(x) + 2s(x)} + \frac{d(x)D_{d\pi^+}(z) + 4\bar{u}(x)D_{u\pi^+}(z) + 2s(x)D_{s\pi^+}(z)}{4u(x) + 4\bar{u}(x) + d(x) + \bar{d}(x) + 2s(x)} \\
M_p^{\pi^-}(x, Q^2, z) &= \frac{4\bar{u}(x)D_{u\pi^-}(z) + d(x)D_{d\pi^-}(z)}{4u(x) + 4\bar{u}(x) + d(x) + \bar{d}(x) + 2s(x)} + \frac{\bar{d}(x)D_{d\pi^-}(z) + 4u(x)D_{u\pi^-}(z) + 2s(x)D_{s\pi^-}(z)}{4u(x) + 4\bar{u}(x) + d(x) + \bar{d}(x) + 2s(x)} \\
M_d^{\pi^+}(x, Q^2, z) &= \frac{[4u(x) + 4d(x)]D_{u\pi^+}(z) + [\bar{u}(x) + \bar{d}(x)]D_{d\pi^+}(z)}{5[u(x) + \bar{u}(x) + d(x) + \bar{d}(x)] + 4s(x)} + \frac{[u(x) + d(x)]D_{d\pi^+}(z) + 2s(x)D_{s\pi^+}(z)}{5[u(x) + \bar{u}(x) + d(x) + \bar{d}(x)] + 4s(x)} + \\
&\quad \frac{[4\bar{u}(x) + 4\bar{d}(x)]D_{u\pi^-}(z) + 2s(x)D_{s\pi^-}(z)}{5[u(x) + \bar{u}(x) + d(x) + \bar{d}(x)] + 4s(x)} \\
M_d^{\pi^-}(x, Q^2, z) &= \frac{[4\bar{u}(x) + 4\bar{d}(x)]D_{u\pi^-}(z) + [u(x) + d(x)]D_{d\pi^-}(z)}{5[u(x) + d(x) + \bar{u}(x) + \bar{d}(x)] + 4s(x)} + \frac{[\bar{u}(x) + \bar{d}(x)]D_{d\pi^-}(z) + 2s(x)D_{s\pi^-}(z)}{5[u(x) + d(x) + \bar{u}(x) + \bar{d}(x)] + 4s(x)} + \\
&\quad \frac{[4u(x) + 4d(x)]D_{u\pi^+}(z) + 2s(x)D_{s\pi^+}(z)}{5[u(x) + d(x) + \bar{u}(x) + \bar{d}(x)] + 4s(x)},
\end{aligned}$$

(S2)

where $s(x) = \bar{s}(x)$ are the strange (s) quark PDF, $D_{u\pi^+}$ and $D_{d\pi^-}$ are the favored FF and $D_{d\pi^+}$ and $D_{u\pi^-}$ are the un-favored FF, respectively, with $u(d)\pi^\pm$ representing $u(d) \rightarrow \pi^\pm$ and $D_{s\pi^+} = D_{s\pi^-}$ are the s quark FF. Note that, under charge symmetry (CS) these reduce to just one favored and one un-favored FF, since CS implies $D_{u\pi^+} = D_{d\pi^-}$ and $D_{u\pi^-} = D_{d\pi^+}$.

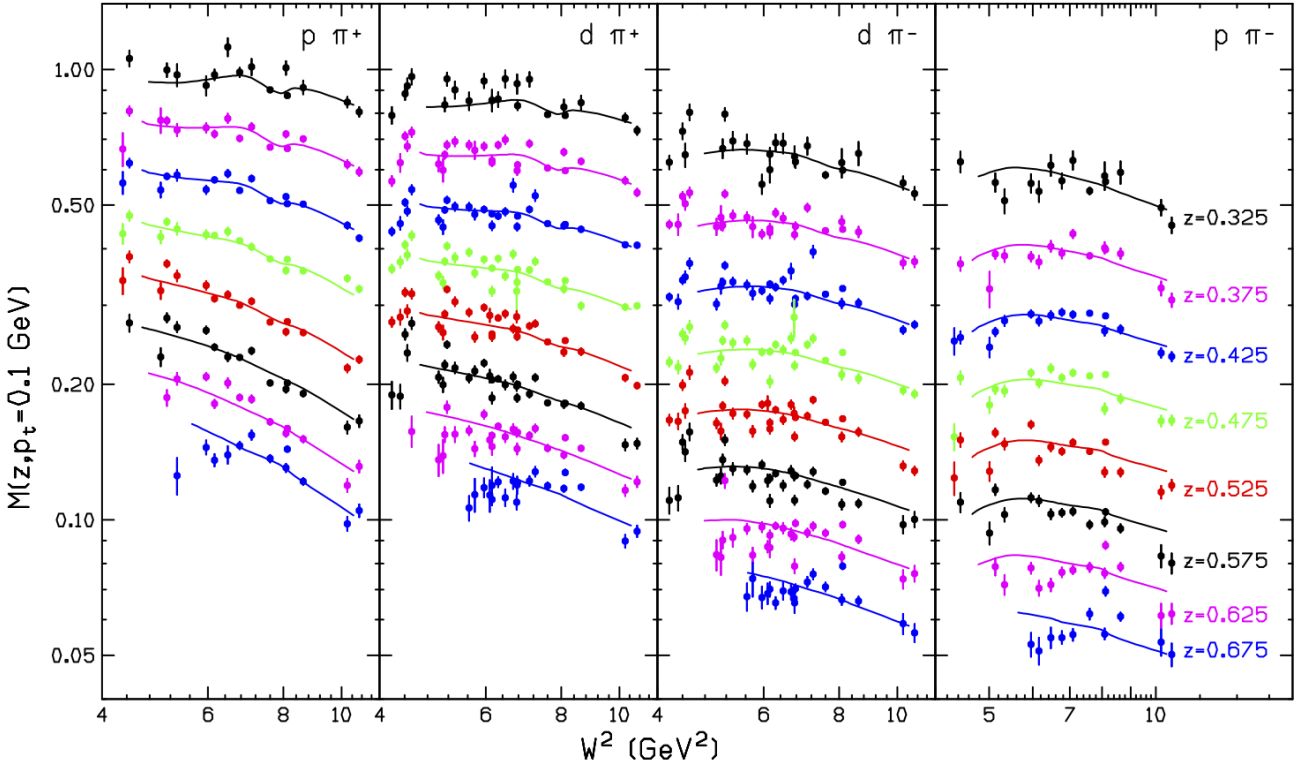


Figure S7: The multiplicities at $p_T = 0.1$ GeV, averaged over ϕ as a function of W^2 for z bins ranging from $z = 0.325$ to 0.675 . From left to right, the panels are for π^+ from a proton target, π^+ from a deuteron target, π^- from a deuteron target, and π^- from a proton target. The solid lines are from the empirical fits. Only the statistical uncertainties are shown. The x and Q^2 bins in Table S3 correspond to average of pairs of points shown here.

Without assuming CS, the four FF as a function of z are extracted from the four multiplicities by simultaneously solving the system of four equations shown above for the eight kinematic settings listed in Table S1. Here we assume that the ratio of longitudinal to transverse cross sections ($R = \sigma_L/\sigma_T$) is flavor independent. The CTEQ5 [S5] PDF were used for u and d quarks while the deFlorian, Sassot, and Stratmann (DSS) [S6, S7] PDF and FF were used for the s quark. These extracted FF as a function of z are shown in Fig. S8 for the eight kinematic settings. They are also compared to two different global fits of existing data, one by DSS [S6, S7] and the other by the Jefferson Lab Angular Momentum collaboration (JAM) [S8] calculated for the highest W (3.2 GeV) setting. Within the experimental uncertainties, the four extracted FF converge to the same values at the lowest x or highest W ,

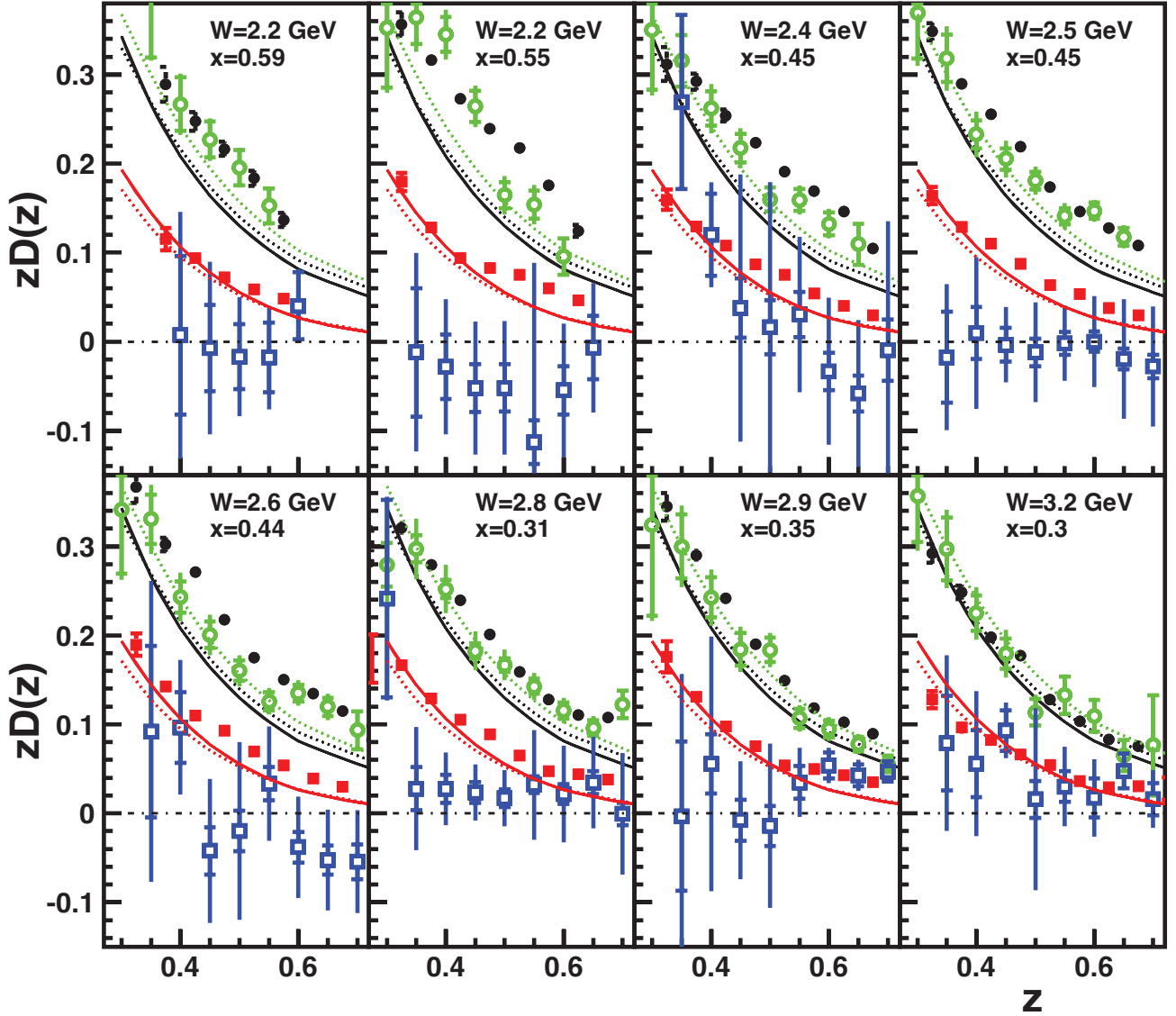


Figure S8: The 4 extracted FF shown as a function of z for the eight kinematic settings. The open (green) and solid (black) circles are the two favored FF, $D_{d\pi^-}$ and $D_{u\pi^+}$, respectively. While the open (blue) and solid (red) squares are the two unfavored FF, $D_{d\pi^+}$ and $D_{u\pi^-}$, respectively. The dashed lines are the results of global fits from DSS [S6, S7], while the solid lines are from the global fit by the JAM collaboration [S8]. Both were calculated for the highest W (3.2 GeV) setting. The JAM collaboration imposes isospin symmetry and hence they produce only one favored FF and one unfavored FF. The inner error bars show the statistical uncertainty while the outer error bars are the total uncertainty which includes the systematic uncertainty in quadrature. The open data points have been shifted relative to the solid points for clarity.

over the entire range of z (0.3 - 0.7). At the lowest x or highest W , they are also in agreement with the global fits. The FF deviate from the global fits as x increases or the W decreases. These results likely point to the importance of higher twist corrections at high x or low W kinematics, which drop off as inverse power laws in W^2 and/or Q^2 . These results when included in fits of world data, will provide an opportunity to estimate higher-order corrections.

The favored and un-favored CSV parameter (δ_{CSV}) extracted from the FF are shown in Fig. S9 for the eight kinematic settings. They are also compared to three different global fits of existing data, one by deFlorian, Sassot, and Stratmann (DSS) [S6, S7], another by the MAP collaboration [S12] and the third by Peng and Ma [S9].

S-III. Systematic Uncertainties

The sources of systematic uncertainties and the total systematic uncertainty of the experiment are listed in Table S2. They have been divided into three categories; normalization/scale uncertainties that impact all measurements equally, point-to-point uncertain-

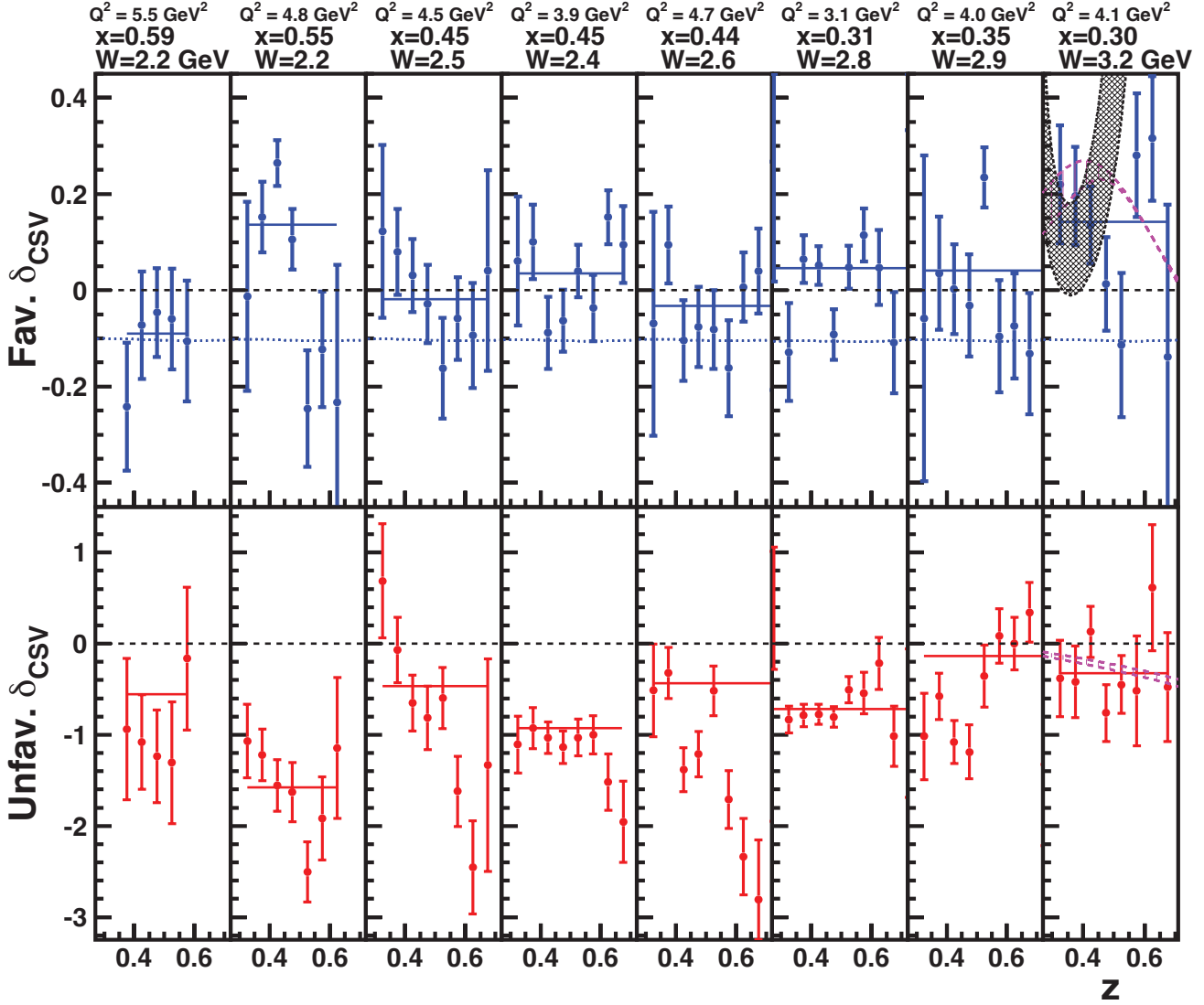


Figure S9: The z dependence of the charge/isospin symmetry violating parameter (δ_{CSV}) for the favored FF (top panels) and un-favored FF (bottom panels), extracted from the measured charged pion multiplicities on hydrogen and deuterium targets. Horizontally, the panels are ordered in decreasing values of x (increasing W). All 8 kinematic settings are shown. Assuming charge symmetry, the δ_{CSV} parameter should be zero, as indicated by the black solid line (top panels). The magenta band with vertical hatching in the last panels is δ_{CSV} and its uncertainty from the global fit by Peng and Ma [S9], the black band with angled hatching is δ_{CSV} and its uncertainty from the global fit by the MAP collaboration [S10], while the dotted lines are from the DSS global fits [S6, S7]. Only statistical uncertainty is shown.

ties that vary with kinematics but are independent of pion species, targets, or z -bins, and correlated uncertainties that can vary with z .

The systematic uncertainty of the charge measurement was determined from the average variation of the charge between data sets collected under similar experimental conditions. The instrumental uncertainty due to electronic noise in the gain monitoring system was also included. There is a 0.7% (0.6%) correlated uncertainty due to uncertainty in the target density for ^1H (^2H), which includes contributions from the uncertainty in the target length, thermal contraction, temperature, pressure, and the equation of state used to calculate the target density. In addition, the uncertainty in the corrections due to local variation in the cryogenic target density was estimated using dedicated scans of the experimental yield with increasing beam current. These scans were carried out before and after the production period of the experiment. The average variation in the current dependence of the measured yield between multiple scans and multiple equivalent analyses along with the residual current dependence of the yield on a carbon foil was used as the systematic uncertainty for the target boiling correction (no current dependent density variation is expected for a carbon foil). The difference in target-density corrections arising from running at different beam currents is estimated to be $<0.25\%$ of the π^+ multiplicity. The systematic uncertainty due to tracking efficiency was determined from the average variation of the efficiency between periods with the same trigger rates. The error in the fit parameters of a linear fit of the rate dependence of the live-time correction is used to estimate the systematic uncertainty due to the live-time correction.

Table S2: Systematic uncertainty of the multiplicities.

Source	Scale Uncertainty (%)	Point-to-Point Uncertainty (%)	Correlated Uncertainty (%)
Charge	-	0.45	-
Target density ^2H (^1H)	0.6 (0.7)	-	-
Target boiling correction	-	0.3	-
Target end cap subtraction	0.1	-	-
Tracking efficiency	-	0.1	-
Live time	-	0.04	-
Particle identification	0.8	-	-
Background subtraction			
ρ^0	-	0.1 - 0.9	0.1- 1.6
Δ	-	< 0.15	0.03 - 0.3
Exclusive	-	< 0.05	0.05 - 0.7
Contamination			
Kaon	-	< 0.1	-
Proton	-	<0.05	-
Electron	-	<0.05	-
Spectrometer Acceptance	1	0.45	-
Kinematics	-	0.2	-
Radiative correction	1	0.5	-
Inclusive cross-section	2	-	-
FADC rate dependence	-	0.9	-
Total	2.65	1.3 - 1.6	0.1-1.8
Total systematic uncertainty added in quadrature = 3.0 to 3.6 %			

The systematic uncertainty in the event selection arising from the particle identification cuts was determined from the average variation in the experimental yield when the cuts were varied by a small fixed amount (typically $\pm 10\%$ of the nominal values) and between multiple equivalent analyses of the same data set. The systematic error on the differential multiplicity between π^+ and π^- is $< 1\%$ of the π^+ multiplicity. It is dominated by the uncertainty in correcting for the residual K^+ contamination in the sample, as determined by performing analyses with different PID cuts and different methods for suppressing the kaon contamination. For example, using a cut on RF timing and heavy-gas Cherenkov vs performing a fit of the RF timing spectrum without the use of heavy-gas Cherenkov counter. The K^- contamination in the π^- sample is typically four times smaller than the K^+ contamination in the π^+ sample and is negligible in comparison. Other sources of systematic error, such as proton/anti-proton and electron/positron contamination in the samples, are also negligible in comparison. All event samples were corrected for kaon contamination and hence the uncertainty due to contamination is small. Differences in rate-dependent corrections were minimized by keeping the single-particle rates the same by adjusting the beam current. The detector efficiencies are similar for π^+ and π^- because all the detectors used in the experiment have similar responses for π^+ and π^- .

The systematic uncertainty of the background subtraction procedure arises from uncertainties in the models used to simulate Δ resonances, exclusive pion production, and ρ^0 meson production. These uncertainties were estimated by varying relevant model parameters by 10% and measuring the corresponding changes in experimental yields. The average variation across eight kinematic settings was used as the z -correlated uncertainty, while the maximum deviation of individual z bins from this average was used as the point-to-point uncertainty. The subtraction of the ρ^0 contribution is a hotly debated topic, therefore, we have listed the multiplicities with and without this subtraction. However, its impact is negligible.

The systematic uncertainty due to radiative correction was estimated from the average variation of the correction factor when the generation limits of the simulation of these radiative processes were varied and when the cross section models in the simulation were varied. Additional details on the models of the radiative processes and their uncertainty can be found in Ref. [S11, S12]. The systematic uncertainty due to the acceptance model in the Monte Carlo simulation was estimated from the variation of the multiplicity when the acceptance cuts were varied. The uncertainty due to the beam energy, spectrometer momentum, and angle settings (i.e. kinematic) was determined from the average variation of the multiplicities when the kinematic settings were varied by the measurement uncertainty of the beam energy, spectrometer momentum, and angles. The uncertainty in the inclusive cross section is from the latest fits to the world data [S12]. The total systematic uncertainty of the measured multiplicity is obtained as the quadrature sum of all uncertainties from the various sources listed in Tab. S2. It ranges from 3.0 to 3.6%

For the sum and difference ratios obtained from the multiplicities, most of these systematic uncertainties cancel to first order and

were found to be negligible compared to the statistical uncertainty of the sum and difference ratios. Only the correlated uncertainty due to target density and the uncertainty due to the inclusive cross section were the major contributions to the sum and difference ratio and led to a 2.2% systematic uncertainty for these ratios.

The systematic uncertainty of the extracted FF arising from the scale/normalization type systematic uncertainties of the multiplicities was studied by scaling the multiplicities and evaluating the variation in the extracted FF. In addition, the change in the extracted FF with the multiple sets of acceptance cuts was also evaluated. From these studies, the systematic uncertainty of the FF was determined to be $\sim 4\%$ for the pair of favored and unfavored FF with the smaller statistical uncertainty. The systematic uncertainty was comparable to or smaller than the statistical uncertainty for the pair of FF with larger statistical uncertainty. The statistical and systematic uncertainty of the unfavored FF, $D_{d\pi^+}(z)$, is significantly larger than all the other FF, because it is determined by the small differences in the flavor-dependent multiplicities, which amplify the uncertainties.

Similarly, the variation in the FF CSV parameters due to the choice of PDF and the scale type uncertainty was used to determine the systematic uncertainties of the δ_{CSV} . They were found to be comparable or smaller than the statistical uncertainties.

S-IV. Results

The four multiplicities, $M_p^{\pi^+}$, $M_d^{\pi^+}$, $M_p^{\pi^-}$ and $M_d^{\pi^-}$ obtained using the π^\pm yield from hydrogen and deuterium targets are listed in Table S3. They include the values with and without the subtraction of the ρ^0 contributions. The statistical uncertainty is also listed. The four fragmentation functions extracted from these four multiplicities are listed in Table S4. These also include the values with and without the subtraction of the ρ^0 contributions.

References

- [S1] H. Mkrтчyan *et al.*, Nucl. Inst. and Meth. A719 (2013) 85
- [S2] S. Ali *et al.* *The Super High Momentum Spectrometer in Hall-C*, publication in preparation
- [S3] T. Horn *et al.*, Nucl. Inst. and Meth. A842 (2017) 28
- [S4] <https://coda.jlab.org>
- [S5] H. L. Lai *et al.*, Phys. Rev. D 55 (1997) 1280
- [S6] D. deFlorian, R. Sassot, M. Stratmann, Phys. Rev. D 75 (2007) 114010
- [S7] D. deFlorian, R. Sassot, M. Epele, R. J. Hernandez-Pinto, M. Stratmann, Phys. Rev. D 91 (2015) 014035
- [S8] E. Moffat, W. Melnitchouk, T. C. Rogers, N. Sato, Phys. Rev. D 104 (2021) 016015
- [S9] Q. Peng, B.-Q. Ma, Phys. Rev. C 107 05 (2023)5202
- [S10] <https://lhpdf.hepforge.org>
- [S11] R. Asaturyan *et al.*, Phys. Rev. C 85 (2012) 015202
- [S12] P. E. Bosted, M. E. Christy, Phys. Rev. C 77 (2008) 065206

Table S3: The four p_T integrated multiplicities at an average $p_T = 0.1$ GeV ($0 < p_T < 0.25$ GeV/c). The multiplicities $M_{p/d}^{\pi^{\pm}}$ ($M_{p/d,\rho}^{\pi^{\pm}}$) are with (without) the ρ^0 contribution subtracted from the pion yields. The Q^2 is in GeV², and W is in GeV.

x	Q^2	W	z	$M_{p,\rho}^{\pi^+}$	$M_p^{\pi^+}$	$\delta M_p^{\pi^+}$	$M_{d,\rho}^{\pi^+}$	$M_d^{\pi^+}$	$\delta M_d^{\pi^+}$	$M_{p,\rho}^{\pi^-}$	$M_p^{\pi^-}$	$\delta M_p^{\pi^-}$	$M_{d,\rho}^{\pi^-}$	$M_d^{\pi^-}$	$\delta M_d^{\pi^-}$
0.59	5.5	2.2	0.375	0.7267	0.7183	0.0369	0.6188	0.6068	0.018	0.3481	0.3395	0.0239	0.4499	0.4383	0.0147
0.59	5.5	2.2	0.425	0.5471	0.5373	0.0176	0.461	0.4483	0.0089	0.2445	0.2358	0.0099	0.3029	0.29	0.0066
0.59	5.5	2.2	0.475	0.4272	0.4185	0.0119	0.3565	0.3448	0.006	0.1709	0.1619	0.006	0.2178	0.2052	0.004
0.59	5.5	2.2	0.525	0.3273	0.3182	0.0116	0.2721	0.26	0.0056	0.1271	0.1192	0.0053	0.1644	0.1523	0.0035
0.59	5.5	2.2	0.575	0.2273	0.2192	0.0099	0.2032	0.1915	0.0053	0.0944	0.0845	0.0048	0.1205	0.1084	0.0032
0.55	4.8	2.2	0.325	1.0241	1.0138	0.0269	0.8679	0.8554	0.023	0.5865	0.5756	0.0205	0.6596	0.6476	0.0246
0.55	4.8	2.2	0.375	0.7835	0.7735	0.0116	0.657	0.6438	0.01	0.3828	0.3718	0.0078	0.4692	0.4555	0.0097
0.55	4.8	2.2	0.425	0.5927	0.5826	0.0077	0.4874	0.4746	0.0065	0.2593	0.2492	0.0046	0.3404	0.3272	0.0056
0.55	4.8	2.2	0.475	0.4633	0.4529	0.007	0.3789	0.3659	0.0057	0.1987	0.1882	0.0038	0.2513	0.2379	0.0043
0.55	4.8	2.2	0.525	0.3744	0.3648	0.0059	0.2876	0.2748	0.0047	0.1545	0.1441	0.0029	0.1778	0.1647	0.0032
0.55	4.8	2.2	0.575	0.2793	0.2687	0.0059	0.2241	0.2119	0.0047	0.1148	0.1044	0.0027	0.1373	0.1241	0.0032
0.55	4.8	2.2	0.625	0.1852	0.1753	0.0072	0.1563	0.1445	0.0056	0.0793	0.0687	0.0034	0.0901	0.0779	0.0037
0.45	3.9	2.4	0.325	0.9437	0.9321	0.0353	0.9262	0.9122	0.0263	0.5393	0.5285	0.0205	0.6129	0.5999	0.021
0.45	3.9	2.4	0.375	0.74	0.7293	0.0146	0.6821	0.6687	0.0106	0.3852	0.3741	0.0075	0.4474	0.4328	0.008
0.45	3.9	2.4	0.425	0.5557	0.5446	0.0094	0.4919	0.4777	0.0065	0.2831	0.2722	0.0044	0.3284	0.3148	0.0047
0.45	3.9	2.4	0.475	0.4348	0.4241	0.0078	0.3801	0.3661	0.0052	0.2053	0.1932	0.0033	0.2397	0.226	0.0035
0.45	3.9	2.4	0.525	0.3377	0.3263	0.0058	0.2994	0.2863	0.004	0.1573	0.146	0.0025	0.1775	0.1642	0.0026
0.45	3.9	2.4	0.575	0.2653	0.2546	0.004	0.2213	0.2078	0.0034	0.1091	0.099	0.002	0.1319	0.1187	0.0022
0.45	3.9	2.4	0.625	0.2075	0.1958	0.0033	0.1666	0.1526	0.0032	0.0764	0.0653	0.0019	0.0949	0.0798	0.0022
0.45	3.9	2.4	0.675	0.1416	0.13	0.0048	0.1203	0.1025	0.0054	0.0534	0.0406	0.0032	0.0682	0.0549	0.0036
0.45	4.5	2.5	0.325	0.9815	0.9717	0.0173	0.8414	0.8287	0.0148	0.5556	0.5448	0.0175	0.6343	0.6215	0.0147
0.45	4.5	2.5	0.375	0.7108	0.7009	0.0085	0.6178	0.6057	0.0073	0.3841	0.3733	0.0076	0.447	0.4346	0.0068
0.45	4.5	2.5	0.425	0.5516	0.5421	0.0049	0.4755	0.4636	0.0042	0.2836	0.2743	0.0039	0.3197	0.3078	0.0035
0.45	4.5	2.5	0.475	0.4216	0.4123	0.0036	0.3609	0.3493	0.003	0.2048	0.1957	0.0027	0.2357	0.2239	0.0024
0.45	4.5	2.5	0.525	0.3037	0.2943	0.0028	0.2618	0.2503	0.0022	0.1394	0.13	0.002	0.1672	0.1553	0.0018
0.45	4.5	2.5	0.575	0.2338	0.2246	0.0023	0.2019	0.1905	0.0017	0.1059	0.0964	0.0017	0.1249	0.1134	0.0015
0.45	4.5	2.5	0.625	0.185	0.1747	0.0022	0.1556	0.1431	0.0015	0.0745	0.064	0.0015	0.0963	0.0836	0.0014
0.45	4.5	2.5	0.675	0.1432	0.1346	0.0023	0.1181	0.1068	0.0016	0.054	0.0459	0.0016	0.0704	0.0593	0.0014
0.44	4.7	2.6	0.325	1.0589	1.0511	0.0332	0.9529	0.9432	0.0273	0.6223	0.614	0.0221	0.6809	0.6708	0.0225
0.44	4.7	2.6	0.375	0.7597	0.7518	0.0116	0.6909	0.6804	0.0099	0.4209	0.4129	0.0072	0.4835	0.4735	0.0077
0.44	4.7	2.6	0.425	0.5789	0.5708	0.007	0.4868	0.4765	0.0058	0.2854	0.2773	0.004	0.3245	0.314	0.0043
0.44	4.7	2.6	0.475	0.4169	0.4087	0.0053	0.3546	0.3447	0.0045	0.2141	0.206	0.003	0.2424	0.2319	0.0033
0.44	4.7	2.6	0.525	0.3101	0.3026	0.0039	0.2763	0.266	0.0034	0.1471	0.1386	0.0021	0.1688	0.1585	0.0023
0.44	4.7	2.6	0.575	0.2347	0.2263	0.0033	0.1938	0.1826	0.0028	0.104	0.0949	0.0017	0.1197	0.1086	0.0019
0.44	4.7	2.6	0.625	0.1909	0.1828	0.0029	0.1536	0.1431	0.0024	0.0753	0.0669	0.0014	0.0945	0.0838	0.0016
0.44	4.7	2.6	0.675	0.1504	0.1414	0.0033	0.1191	0.108	0.0026	0.0554	0.0471	0.0014	0.0719	0.0613	0.0016
0.44	4.7	2.6	0.725	0.1161	0.1069	0.0065	0.1029	0.093	0.005	0.0457	0.0366	0.0029	0.057	0.0469	0.003
0.31	3.1	2.8	0.275	1.0606	1.0446	0.0363	1.0346	1.0144	0.0303	0.72	0.702	0.0449	0.802	0.7777	0.0399
0.31	3.1	2.8	0.325	0.8877	0.8734	0.0068	0.794	0.7765	0.0055	0.5525	0.5383	0.0064	0.5914	0.5742	0.0061
0.31	3.1	2.8	0.375	0.6704	0.6573	0.0039	0.6002	0.5839	0.0031	0.3928	0.3791	0.0034	0.4408	0.4247	0.0033
0.31	3.1	2.8	0.425	0.5074	0.4951	0.0025	0.454	0.4393	0.002	0.2855	0.2731	0.0021	0.3226	0.3077	0.002
0.31	3.1	2.8	0.475	0.3797	0.368	0.002	0.339	0.3247	0.0015	0.2097	0.1976	0.0015	0.2314	0.217	0.0014
0.31	3.1	2.8	0.525	0.2753	0.2637	0.0017	0.2495	0.2354	0.0013	0.1457	0.1339	0.0012	0.1665	0.1521	0.0012
0.31	3.1	2.8	0.575	0.2014	0.1897	0.0017	0.1817	0.1675	0.0014	0.1012	0.0894	0.0013	0.1188	0.1049	0.0012
0.31	3.1	2.8	0.625	0.1619	0.1502	0.0018	0.1488	0.1345	0.0016	0.0836	0.0714	0.0013	0.0958	0.0813	0.0011
0.31	3.1	2.8	0.675	0.141	0.1289	0.0016	0.1241	0.1095	0.0014	0.0664	0.054	0.0011	0.0757	0.0614	0.001
0.31	3.1	2.8	0.725	0.1055	0.0925	0.0025	0.0933	0.0793	0.0021	0.0485	0.0365	0.002	0.0625	0.0478	0.0015
0.35	4.0	2.9	0.325	0.9554	0.9467	0.0239	0.8369	0.8247	0.0221	0.5873	0.578	0.0263	0.6392	0.6287	0.0292
0.35	4.0	2.9	0.375	0.709	0.7006	0.0081	0.6389	0.6287	0.0077	0.3953	0.3867	0.0079	0.4461	0.4353	0.0089
0.35	4.0	2.9	0.425	0.5111	0.5027	0.0048	0.4456	0.4351	0.0049	0.2642	0.2555	0.0043	0.3028	0.2919	0.0049
0.35	4.0	2.9	0.475	0.3577	0.3484	0.0038	0.3098	0.2989	0.0044	0.1817	0.1726	0.0032	0.2078	0.1965	0.0036
0.35	4.0	2.9	0.525	0.2609	0.2516	0.0028	0.2363	0.2256	0.0033	0.1276	0.1186	0.0021	0.1552	0.144	0.0024
0.35	4.0	2.9	0.575	0.1927	0.1837	0.0022	0.1798	0.1688	0.0023	0.0971	0.088	0.0016	0.1086	0.0974	0.0018
0.35	4.0	2.9	0.625	0.1531	0.144	0.002	0.1422	0.1311	0.0015	0.0775	0.0682	0.0012	0.087	0.0761	0.0014
0.35	4.0	2.9	0.675	0.1252	0.1158	0.0017	0.1178	0.1062	0.0013	0.0589	0.0493	0.001	0.0662	0.0547	0.0012
0.35	4.0	2.9	0.725	0.1082	0.0993	0.002	0.0908	0.0792	0.0012	0.0457	0.0363	0.0011	0.0499	0.0382	0.0012
0.35	4.0	2.9	0.775	0.0821	0.0735	0.0039	0.07	0.0601	0.0019	0.0333	0.0235	0.0022	0.0395	0.0299	0.0021
0.30	4.1	3.2	0.325	0.8251	0.8152	0.015	0.7552	0.7441	0.012	0.4705	0.4599	0.0134	0.5447	0.5324	0.0128
0.30	4.1	3.2	0.375	0.6041	0.5951	0.0093	0.5492	0.5383	0.0074	0.3167	0.3078	0.008	0.3734	0.3606	0.0075
0.30	4.1	3.2	0.425	0.4354	0.4268	0.0049	0.408	0.3982	0.004	0.2325	0.2241	0.0041	0.2682	0.2585	0.0037
0.30	4.1	3.2	0.475	0.3342	0.3258	0.004	0.2982	0.2878	0.0032	0.1662	0.1574	0.0032	0.192	0.1816	0.0028
0.30	4.1	3.2	0.525	0.2224	0.2148	0.003	0.2025	0.1939	0.0024	0.1174	0.1097	0.0025	0.13	0.1209	0.0021
0.30	4.1	3.2	0.575	0.1633	0.156	0.0035	0.1473	0.1389	0.0028	0.0814	0.0738	0.0031	0.0991	0.0902	0.0029
0.30	4.1	3.2	0.625	0.1256	0.1182	0.0029	0.119	0.1103	0.0023	0.0617	0.0545	0.0024	0.0751	0.0659	0.0023
0.30	4.1	3.2	0.675	0.1017	0.0947	0.0025	0.0922	0.0843	0.002	0.0515	0.0447	0.0023	0.0572	0.0481	0.002
0.30	4.1	3.2	0.725	0.0878	0.0809	0.0042	0.0746	0.0656	0.0029	0.0456	0.0365	0.0082	0.0527	0.0453	0.0045

Table S4: The four fragmentation functions extracted from the four multiplicities. The FF $D_{u/d\pi^\pm}$ ($D_{u/d\pi^\pm}^\rho$) are obtained with (without) the ρ^0 contribution subtracted from the multiplicities. The Q^2 is in GeV^2 , and W is in GeV .

x	Q^2	W	z	$zD_{u\pi^+}^\rho$	$zD_{u\pi^+}$	$\delta zD_{u\pi^+}$	$zD_{d\pi^+}^\rho$	$zD_{d\pi^+}$	$\delta zD_{d\pi^+}$	$zD_{u\pi^-}^\rho$	$zD_{u\pi^-}$	$\delta zD_{u\pi^-}$	$zD_{d\pi^-}^\rho$	$zD_{d\pi^-}$	$\delta zD_{d\pi^-}$
0.59	5.5	2.2	0.375	0.2916	0.2889	0.0195	0.1180	0.1152	0.0127	0.0190	0.0071	0.0891	0.3917	0.3812	0.0619
0.59	5.5	2.2	0.425	0.2511	0.2474	0.0105	0.0969	0.0938	0.0060	0.0048	-0.0073	0.0486	0.2819	0.2667	0.0300
0.59	5.5	2.2	0.475	0.2202	0.2166	0.0080	0.0758	0.0721	0.0040	-0.0037	-0.017	0.0367	0.2424	0.2271	0.0203
0.59	5.5	2.2	0.525	0.1878	0.1836	0.0085	0.0621	0.0587	0.0040	-0.0031	-0.018	0.0391	0.2136	0.1952	0.0198
0.59	5.5	2.2	0.575	0.1404	0.1365	0.0080	0.0535	0.0482	0.0039	0.0583	0.0403	0.0376	0.1665	0.1526	0.0195
0.55	4.8	2.2	0.325	0.3596	0.3566	0.0132	0.1827	0.1793	0.0103	-0.004	-0.0121	0.0722	0.3581	0.3522	0.0671
0.55	4.8	2.2	0.375	0.3194	0.3161	0.0065	0.1319	0.1282	0.0046	-0.0167	-0.0284	0.0361	0.3751	0.3642	0.0301
0.55	4.8	2.2	0.425	0.2767	0.2729	0.0049	0.0978	0.0940	0.0030	-0.0403	-0.0522	0.0267	0.3580	0.3451	0.0198
0.55	4.8	2.2	0.475	0.2433	0.2389	0.0050	0.0870	0.0826	0.0028	-0.0388	-0.052	0.0268	0.2784	0.2642	0.0175
0.55	4.8	2.2	0.525	0.2221	0.2178	0.0046	0.0800	0.0751	0.0023	-0.0968	-0.113	0.0247	0.1792	0.1643	0.0146
0.55	4.8	2.2	0.575	0.1812	0.1755	0.0051	0.0650	0.0597	0.0024	-0.0425	-0.0547	0.0271	0.1706	0.1539	0.0156
0.55	4.8	2.2	0.625	0.1301	0.1244	0.0068	0.0524	0.0462	0.0033	0.0073	-0.0068	0.0357	0.1087	0.0954	0.0203
0.45	3.9	2.4	0.325	0.3151	0.3118	0.0192	0.1625	0.1594	0.0115	0.2787	0.2692	0.0980	0.3586	0.3499	0.0671
0.45	3.9	2.4	0.375	0.2956	0.2922	0.0091	0.1325	0.1291	0.0049	0.1315	0.1201	0.0462	0.3293	0.3155	0.0289
0.45	3.9	2.4	0.425	0.2579	0.2539	0.0067	0.1117	0.1077	0.0033	0.0519	0.0375	0.0332	0.2748	0.2617	0.0193
0.45	3.9	2.4	0.475	0.2278	0.2236	0.0062	0.0920	0.0867	0.0028	0.0327	0.0161	0.0303	0.2286	0.2173	0.0161
0.45	3.9	2.4	0.525	0.1962	0.1907	0.0051	0.0807	0.0753	0.0023	0.0430	0.0304	0.0252	0.1735	0.1598	0.0133
0.45	3.9	2.4	0.575	0.1741	0.1689	0.0039	0.0588	0.0540	0.0020	-0.0155	-0.0335	0.0208	0.1779	0.1590	0.0123
0.45	3.9	2.4	0.625	0.1526	0.1461	0.0036	0.0456	0.0401	0.0021	-0.0405	-0.0583	0.0202	0.1577	0.1324	0.0127
0.45	3.9	2.4	0.675	0.1105	0.1050	0.0056	0.0379	0.0295	0.0037	0.0288	-0.0098	0.0344	0.1203	0.1093	0.0230
0.45	4.5	2.5	0.325	0.3508	0.3482	0.0095	0.1671	0.1640	0.0096	-0.0075	-0.0176	0.0512	0.3777	0.3694	0.0514
0.45	4.5	2.5	0.375	0.2923	0.2891	0.0054	0.1324	0.1287	0.0049	0.0194	0.0096	0.0290	0.3266	0.3181	0.0265
0.45	4.5	2.5	0.425	0.2589	0.2554	0.0035	0.1136	0.1103	0.0029	0.0079	-0.0036	0.0189	0.2449	0.2328	0.0156
0.45	4.5	2.5	0.475	0.2228	0.2190	0.0029	0.0911	0.0875	0.0022	0.0004	-0.012	0.0155	0.2188	0.2051	0.0121
0.45	4.5	2.5	0.525	0.1781	0.1738	0.0025	0.0678	0.0636	0.0018	0.0111	-0.0019	0.0129	0.1953	0.1807	0.0099
0.45	4.5	2.5	0.575	0.1510	0.1464	0.0022	0.0584	0.0536	0.0017	0.0145	-0.0001	0.0113	0.1549	0.1410	0.0091
0.45	4.5	2.5	0.625	0.1333	0.1276	0.0023	0.0435	0.0377	0.0016	-0.0031	-0.0196	0.0116	0.1637	0.1470	0.0091
0.45	4.5	2.5	0.675	0.1124	0.1076	0.0026	0.0336	0.0293	0.0019	-0.0088	-0.028	0.0129	0.1381	0.1178	0.0099
0.44	4.7	2.6	0.325	0.3689	0.3667	0.0182	0.1919	0.1895	0.0124	0.0991	0.0920	0.0963	0.3482	0.3412	0.0720
0.44	4.7	2.6	0.375	0.3044	0.3020	0.0074	0.1451	0.1425	0.0047	0.1068	0.0966	0.0396	0.3390	0.3305	0.0278
0.44	4.7	2.6	0.425	0.2741	0.2712	0.0050	0.1131	0.1102	0.0030	-0.0318	-0.0422	0.0267	0.2539	0.2429	0.0176
0.44	4.7	2.6	0.475	0.2205	0.2171	0.0043	0.0960	0.0928	0.0025	-0.0098	-0.0197	0.0229	0.2128	0.2005	0.0149
0.44	4.7	2.6	0.525	0.1777	0.1746	0.0035	0.0734	0.0695	0.0019	0.0482	0.0334	0.0188	0.1719	0.1604	0.0116
0.44	4.7	2.6	0.575	0.1540	0.1501	0.0032	0.0583	0.0537	0.0017	-0.0214	-0.0381	0.0170	0.1395	0.1258	0.0102
0.44	4.7	2.6	0.625	0.1385	0.1343	0.0031	0.0437	0.0393	0.0015	-0.0363	-0.0525	0.0164	0.1511	0.1352	0.0093
0.44	4.7	2.6	0.675	0.1204	0.1151	0.0037	0.0348	0.0301	0.0017	-0.0378	-0.0544	0.0194	0.1368	0.1197	0.0103
0.44	4.7	2.6	0.725	0.0970	0.0906	0.0079	0.0339	0.0277	0.0037	0.0252	0.0147	0.0409	0.1053	0.0933	0.0213
0.31	3.1	2.8	0.275	0.3032	0.3000	0.0216	0.1773	0.1740	0.0270	0.2563	0.2415	0.1109	0.4113	0.3906	0.1414
0.31	3.1	2.8	0.325	0.3243	0.3207	0.0048	0.1702	0.1665	0.0046	0.0418	0.0277	0.0242	0.2930	0.2795	0.0245
0.31	3.1	2.8	0.375	0.2830	0.2792	0.0031	0.1332	0.1289	0.0029	0.0433	0.0275	0.0159	0.3106	0.2973	0.0153
0.31	3.1	2.8	0.425	0.2440	0.2397	0.0023	0.1095	0.1052	0.0019	0.0379	0.0234	0.0116	0.2670	0.2521	0.0104
0.31	3.1	2.8	0.475	0.2054	0.2010	0.0020	0.0936	0.0889	0.0016	0.0339	0.0172	0.0100	0.1982	0.1825	0.0085
0.31	3.1	2.8	0.525	0.1639	0.1591	0.0019	0.0700	0.0651	0.0014	0.0501	0.0321	0.0094	0.1853	0.1667	0.0076
0.31	3.1	2.8	0.575	0.1334	0.1280	0.0021	0.0533	0.0477	0.0016	0.0416	0.0218	0.0109	0.1604	0.1427	0.0084
0.31	3.1	2.8	0.625	0.1161	0.1103	0.0024	0.0505	0.0442	0.0017	0.0566	0.0346	0.0126	0.1362	0.1155	0.0091
0.31	3.1	2.8	0.675	0.1141	0.1075	0.0024	0.0453	0.0382	0.0017	0.0229	-0.0006	0.0126	0.1159	0.0958	0.0087
0.31	3.1	2.8	0.725	0.0944	0.0857	0.0040	0.0318	0.0249	0.0031	0.0194	0.0032	0.0203	0.1487	0.1223	0.0154
0.35	4.0	2.9	0.325	0.3465	0.3446	0.0155	0.1786	0.1759	0.0176	0.0090	-0.0033	0.0838	0.3308	0.3245	0.1024
0.35	4.0	2.9	0.375	0.2924	0.2898	0.0061	0.1337	0.1311	0.0061	0.0643	0.0555	0.0332	0.3102	0.3000	0.0360
0.35	4.0	2.9	0.425	0.2449	0.2421	0.0041	0.1006	0.0976	0.0038	0.0033	-0.0077	0.0232	0.2542	0.2427	0.0224
0.35	4.0	2.9	0.475	0.1940	0.1902	0.0038	0.0787	0.0752	0.0032	-0.0033	-0.0141	0.0223	0.1974	0.1843	0.0186
0.35	4.0	2.9	0.525	0.1531	0.1488	0.0031	0.0579	0.0541	0.0023	0.0460	0.0348	0.0184	0.1982	0.1837	0.0136
0.35	4.0	2.9	0.575	0.1224	0.1181	0.0026	0.0539	0.0496	0.0019	0.0686	0.0538	0.0146	0.1222	0.1068	0.0110
0.35	4.0	2.9	0.625	0.1071	0.1024	0.0024	0.0479	0.0429	0.0016	0.0591	0.0429	0.0123	0.1090	0.0948	0.0093
0.35	4.0	2.9	0.675	0.0949	0.0897	0.0023	0.0405	0.0350	0.0014	0.0658	0.0470	0.0113	0.0952	0.0779	0.0083
0.35	4.0	2.9	0.725	0.0947	0.0898	0.0028	0.0356	0.0301	0.0016	-0.0004	-0.0232	0.0133	0.0765	0.0557	0.0094
0.35	4.0	2.9	0.775	0.0780	0.0721	0.0057	0.0291	0.0214	0.0034	0.0040	-0.0111	0.0256	0.0702	0.0638	0.0187
0.30	4.1	3.2	0.325	0.2950	0.2922	0.0105	0.1307	0.1278	0.0096	0.0858	0.0790	0.0530	0.3651	0.3565	0.0518
0.30	4.1	3.2	0.375	0.2511	0.2485	0.0075	0.0984	0.0965	0.0066	0.0658	0.0559	0.0378	0.3139	0.2972	0.0352
0.30	4.1	3.2	0.425	0.2012	0.1980	0.0045	0.0855	0.0825	0.0038	0.1015	0.0931	0.0228	0.2335	0.2248	0.0199
0.30	4.1	3.2	0.475	0.1801	0.1770	0.0041	0.0694	0.0660	0.0033	0.0284	0.0157	0.0207	0.1906	0.1794	0.0172
0.30	4.1	3.2	0.525	0.1318	0.1283	0.0034	0.0577	0.0544	0.0029	0.0388	0.0300	0.0172	0.1245	0.1137	0.0148
0.30	4.1	3.2	0.575	0.1073	0.1037	0.0043	0.0400	0.0363	0.0039	0.0273	0.0174	0.0218	0.1441	0.1328	0.0212
0.30	4.1	3.2	0.625	0.0871	0.0833	0.0039	0.0329	0.0296	0.0034	0.0598	0.0477	0.0197	0.1256	0.1096	0.0180
0.30	4.1	3.2	0.675	0.0798	0.0757	0.0036	0.0337	0.0306	0.0034	0.0264	0.0160	0.0182	0.0840	0.0652	0.0175
0.30	4.1	3.2	0.725	0.0773	0.0737	0.0064	0.0357	0.0279	0.0123	0.0000	-0.0188	0.0308	0.0722	0.0765	0.0564